University of Tartu

Faculty of Science and Technology

Institute of Ecology and Earth Sciences

Department of Geology

Imre Andreas Martin

Palaeozoic carbon isotope anomalies and sample-scale component analysis

MSc thesis

Supervisors: Leho Ainsaar

Aivo Lepland

TARTU 2022

Palaeozoic carbon isotope anomalies and sample-scale component analysis

Studies of the carbon isotope composition of Palaeozoic carbonate sedimentary rocks have focused almost exclusively on bulk-rock analysis to reconstruct palaeoclimate, assuming limited sample-scale isotopic heterogeneity. However, several studies have shown that $\delta^{13}C$ values of individual components can vary a great deal compared to bulk-rock. Particular attention has been paid to the positive $\delta^{13}C$ excursions, that are likely to reflect specific climatic events. This thesis focuses on two largest Palaeozoic $\delta^{13}C$ excursions, the Hirnantian Isotopic Carbon Excursion (HICE) in the end of the Ordovician Period and the Mid-Ludfordian Carbon Isotope Excursion (MLCIE) in the Silurian Period. Previous bulk-rock investigations have demonstrated the occurrance of distinct carbonate sections with high $\delta^{13}C$ values in the Baltic region cross-sections, which stratigraphically correspond to HICE and MLCIE intervals. To investigate the sample-scale variability of the isotopic composition of these high $\delta^{13}C$ rocks and guided by the previous bulk-rock results, three samples were selected from the HICE interval (Karinu and Kamariku drill cores in the Pandivere region of North Estonia and Otepää drill core in South Estonia) and two samples from MLCIE (Vidukle drill core of Central Lithuania). The results obtained by mass spectrometery (IRMS and SIMS) anlaysis performed on the sample-scale material, show that deviation of different rock component composition from average and bulk-rock value increases with the increase of lithological heterogeneity. Limited sample-scale heterogeneity and good correspondence with bulk-rock $\delta^{13}C$ values is seen in micritic samples whereas wacke- and grainstone samples exhibit up to 5‰ range of $\delta^{13}C$ values with several components up to 3‰ heavier than the bulk-rock values. Lithologic variability and isotopic heterogeneity of wacke- and grainstone smaples should thus be accounted in reconstruction of $\delta^{13}C$ curves, which would most accurately reflect depositional conditions at that time. About 3‰ $\delta^{18}O$ variance in distinct components is also seen in one lithologically heterogeneous sample (OP) and combined with trace elements data, the results indicate that oxygen isotopic signals are commonly diagenetically overprinted, but some components may preserve primary signatures. In addition, enrichment (∼1 ‰) with ^{18}O can be seen in HMG materials, consistent with previous studies.

Keywords: Carbonate rocks, carbon isotopes, oxygen isotopes, component analysis, Baltic basin

P420 petrology, mineralogy, geochemistry

Paleosoikumi süsiniku isotoopanomaaliad ja proovi-skaalas komponentanalüüs

Paleosoikumi karbonaatsete settekivimite süsinuku isotoopkoostise uuringud on peaaegu eranditult keskendunud täiskivimi analüüsidele, et rekonstrueerida paleokliimat, eeldades isotoopkoostise piiratud heterogeensust proovi-skaalas. Mitmed uuringud on aga näidanud, et erinevate kivimi komponentide $\delta^{13}C$ väärtused võivad võrreldes täiskivimiga oluliselt erineda. Erilist tähelepanu on pööratud positiivsetele $\delta^{13}C$ ekskursioonide uurimisele, mis tõenäoliselt peegeldavad kindlaid kliimasündmusi. Antud töö keskendub kahele suurimale Paleosoikumi $\delta^{13}C$ ekskursioonile, Hirnanti Süsiniku Isotoobi Ekskursioon (HICE) Ordoviitsiumi ajastu lõpus ja Kesk-Ludfordi Süsiniku Isotoobi Ekskursioon (MLCIE) Siluri ajastul. Varasemad täiskivimi uuringud on näidanud kõrgete $\delta^{13}C$ väärtustega karbonaatkivimite intervallide esinemist Balti piirkonna läbilõigetes, mis stratigraafiliselt vastavad HICE ja MLCIE esinemise tasemetele. Uurimaks nende kõrge $\delta^{13}C$ väärtusega kivimite isotoopkoostise homogeensust, valiti eelnevalt teostatud täiskivimi analüüside tulemuste põhjal kaks proovi, Põhja-Eesti Pandivere piirkonna Karinu ja Kamariku puursüdamike HICE intervallis, üks proov Lõuna-Eesti Otepää südamiku HICE intervallist ja kaks proovi Kesk-Leedu Vidukle puursüdamiku MLICE intervallist. Prooviskaalas teostatud mass-spektromeetriliste (IRMS ja SIMS) analüüside tulemused näitavad, et isegi väikestest proovidest saadud erinevate kivimkomponentide koostise hajuvus keskmisest ning täiskivimi väärtusest suureneb koos analüüsitud materjalide litoloogilise heterogeensuse suurenenemisega. Piiratud heterogeensust proovi-skaalas ja head vastavust täiskivimi $\delta^{13}C$ väärtustega on näha mikriitsetes proovides, samas kui mudalis-teraliste ja teraliste lubjakiviproovide $\delta^{13}C$ väärtuste vahemik on kuni 5‰ ning mitmete komponentide väärtused on kuni 3‰ raskemad kui täiskivimi väärtused. Litoloogiliselt erinevatele proovidele tehtud uuringu tulemusena on võimalik anda enne proovide analüüsimist hinnang, vähendades proovide arvu ning samal ajal säilitades andmete usalduväärsust, et rekonstrueerida $\delta^{13}C$ kõveraid, mis võiksid täpsemini peegeldada settimisaegseid tingimusi. Umbes 3‰ $\delta^{18}O$ varieeruvust on näidatud litoloogiliselt kõige heterogeensemas Otepää proovis ning saadud kombineeritud andmed kinnitavad, et isotoopsignaalid ei ole täielikult diageneesist mõjutatud. Lisaks võib kõrge magneesiumi sialdusega materjalides näha ^{18}O-ga rikastumist (∼1‰), mida toetavad ka varasemad uuringud.

Märksõnad: Karbonaatkivimid, süsiniku isotoobid, hapniku isotoobid, komponentanalüüs, Balti bassein

P420 petroloogia, mineraloogia, geokeemia

Table of Contents

1. Introduction

Carbon and oxygen isotope ratios have been used to reconstruct palaeoclimate over past geological times. Stable carbon and oxygen isotopic ratio curves constructed from marine carbonates through time, show variations that can be used for stratigraphic correlation, reconstructing global carbon cycle dynamics and palaeo-temperatures. Palaeozoic $\delta^{13}C$ studies have almost exclusively focused on bulk-rock analysis, assuming limited sample-scale isotopic heterogeneity. Several studies have, however provided isotopic data from specific rock components and the results have shown that $\delta^{13}C$ values of individual components can vary a great deal compared to bulk-rock (Cramer & Jarvis, 2020). Despite the awareness of possible sample-scale isotopic heterogeneity, the bulk-rock datasets remain important source of information for palaeoenvironmental studies and chemostratigraphic correlations. (Cramer & Jarvis, 2020 ; Grossman & Joachimski, 2020)

Particular attention has been paid to the positive $\delta^{13}C$ excursions, which likely reflect climatic events. This thesis focuses on two largest Palaeozoic $\delta^{13}C$ excursions, the Hirnantian Isotopic Carbon Excursion (HICE) in the end of the Ordovician period and the Mid-Ludfordian Carbon Isotope Excursion (MLCIE) in the Silurian period. The studied materials include four lithologically variable Ordovician HICE samples collected from cores Kamariku-5, Karinu-1 (Ainsaar, Truumees, & Meidla, 2015) and Otepää (Oraspõld, 1975) drilled in Estonia. Two Silurian MLCIE samples are taken from Lithuanian drill core Vidukle-61 (Martma, *et al.,* 2005).

Estonian Ordovician successions are among least altered in the world where marine fauna is well preserved (Nõlvak, 1997) whereas Lithuanian Vidukle-61 core is considered to provide one of the most complete geological section of the Silurian (Spiridonov, *et al.,* 2020). Previous bulk-rock investigations have demonstrated the occurrance of distinct carbonate intervals with high $\delta^{13}C$ values in these drill cores corresponding to HICE and MLCIE. Guided by the previous bulk-rock results, samples from these excursion intervals were selected for the study of sample-scale isotopic heterogeiety.

Individual components in all samples were petrographically characterized and geochemically studied, using micro-drilled sub-samples and different in-situ methods. The thesis aims at characterization of isotopic and elemental heterogeneity of individual components in carbonate rocks. The component specific results are used to assess of which components

carry the primary depositional isotopic signatures and which components are not representative of primary environment due to isotopic resetting and/or diagenetic fromation. The comparison of bulk-rock and component specific data allows to assess the reliability of bulk-rock data for environmental reconstructions and offers an opportunity to refine interpretations of magnitudes of $\delta^{13}C$ excursions and related dynamics of seawater dissolved inorganic carbon (DIC).

2. Carbon and oxygen stable isotopes as tool for palaeoenvironmental reconstruction and stratigraphical correlation of marine carbonates

Analysis of carbon (C) isotope ratios ($^{13}C/^{12}C$) in marine carbonates and organic matter (OM) has been a key tool for providing insights into past ocean-atmosphere chemistry, climate and evolving environmental conditions over past decades. Geological carbon cycle ties together the ocean-atmosphere carbon pool, Earth's biosphere and sedimentary reservoirs. (Bachan, *et al.,* 2017). Over the past two decades increasingly higher resolution carbon isotope data and their detailed integration with biostratigraphy have significantly improved global stratigraphic correlations. (Cramer & Jarvis, 2020)

Variations in the oxygen (O) isotope ratios ($^{18}O/^{16}O$) in marine carbonates, fossils and microfossils have enabled reconstruction of palaeotemperatures of Phanerozoic oceans. At sedimentary temperatures the $\delta^{18}O$ of a carbonate is inversely correlated to temperature and the relationship is approximately 4° C for every change of 1‰ in the value of $\delta^{18}O$ (Swart, 2015). Therefore, oxygen isotope stratigraphy is another way to derive insight into Earth's palaeoclimate. Oxygen isotope events of Palaeozoic age, mark local and global climate change and these events serve as chemostratigraphic markers for global and regional correlation. (Grossman & Joachimski, 2020)

2.1 Bulk rock isotopic composition

Carbonate minerals which can form through a variety of abiotic, biotic and biologically mediated processes, can be sampled and analysed for $\delta^{13}C_{carb}$. Comparing time equivalent $\delta^{13}C_{carb}$ values of pelagic and benthic calcifying organisms gives an opportunity to assess isotopic gradients with depth and overall spatial heterogeneity of $\delta^{13}C$ in the global ocean. (Cramer & Jarvis, 2020). Palaeoenvironmental reconstructions using isotope data from carbonate minerals need, however, to account for diagenetic precipitation and re-crystallization, hence the robust approach to determine isotopic composition of ancient oceans has been to use diagenetically „stable" low-Mg calcite components (Brand, 1982). For Palaeozoic reconstructions, the well-preserved portions of brachiopods have been used (Popp, Anderson, & Sandberg, 1986). For $\delta^{18}O$ values, articulate brachiopods shells are also favoured over other rock components based on resistance to diagenesis and tendency for

inner shell layers to be precipitated near oxygen isotope equilibrium with ambient water (Grossman & Joachimski, 2020).

One of the factors that needs to be considered with brachiopods is their shell size as thicker and denser shells retain original isotopic composition better (Grossman, *et al.,* 2008). Interpretation of $\delta^{13}C$ data of individual species or groups of species is complicated due to fact that biocalcification can impart a fractionation that can mask the original marine DIC $\delta^{13}C$ value. Moreover the limited presence of brachiopods in any given stratigraphic interval affects stratigraphic resolution. Therefore, over the past decade, Palaeozoic $\delta^{13}C$ studies have become almost exclusively focused on sampling bulk carbonate. Bulk-rock carbonate sampling typically targets fine-grained, primarily micritic carbonate and utmost care is taken to avoid secondary calcite void infills or veins. Major drawback to bulk sampling is the inability to target specific carbonate components, which however can be isolated by micro-drilling. Bulk sampling can be carried out by using disk mill or ball mill to generate large amounts of powder but this is usually only done to generate enough material to analyse different isotope proxies like Sr, S or organic carbon from same sample powder. (Cramer & Jarvis, 2020) In this thesis, bulk-rock is referred to powders (1–2 g) generated from studied samples (before thin sections were made) using a drill with a large drill bit.

Identification and correlation of positive and negative excursions is one of the primary functions of $\delta^{13}C$ stratigraphy to the geological time scale. Through integration with bio-, magneto- or chronostratigraphic tool these excursions can be verified to be globally significant chronostratigraphic markers. (Cramer & Jarvis, 2020). Constructed $\delta^{13}C_{carb}$ curves through Phanerozoic time, exhibit relatively low (-1‰ to +4‰) amplitude variations from Mid-Jurassic through Cenozoic, compared to earlier part of the Phanerozoic record (variations from -3 to +8‰) (Saltzman & Thomas, 2012). Given the diagenetic resistance of brachiopods, diagenetically modified bulk carbonate can be around 2‰ lower in $\delta^{18}O$ than co-occurring brachiopods (Veizer, *et al.,* 1999). Therefore, $\delta^{18}O$ curves are constructed mainly from brachiopod data exhibiting common $\delta^{18}O$ values from -10‰ to -4‰ for Cambrian and Ordovician, -8‰ to -2‰ for Silurian and Devonian and -7‰ to 0‰ for Carboniferous and Permian (Grossman & Joachimski, 2020).

The global biochemical cycle of carbon involving a complex interplay of abiotic and biological reactions that fractionate carbon isotopes, play key role in regulating Earth's climate. In

marine record secular variation is shown in the carbon isotope composition. Throughout the Phanerozoic, the size of ocean reservoirs and carbon fluxes have changed significantly. (Frýda, *et al.,* 2021) Removal or addition of either ^{12}C or ^{13}C from the environment during specific time intervals can change the isotopic composition of marine DIC and result in carbon isotope excursions (CIE) as recorded in rock record (Cramer & Jarvis, 2020). Kump and Arthur, (1999) have given a general overview on how to interpret CIEs. They concluded that when considering the isotopic mass-balance constraints imposed on the ocean-atmosphere system and influence on isotopic composition of organic matter (OM) imposed by changes in pCO_2, then increased burial of organic carbon leads to fall in atmospheric pCO_2, which causes a positive excursion in both inorganic and organic carbon. Relative to organic carbon and silicate weathering, an increase in the proportion of carbonate weathering can also drive a large positive excursion in the isotopic composition of the ocean. Only small changes in carbon isotopic composition of the marine DIC and limestones deposited from it, can be explained by increased volcanism or decreased silicate weathering if associated drawdown in atmospheric pCO_2 affects the photosynthetic isotopic effect. A significant change in the terrestrial vegetation, like increase in the proportion of C_4 plant-derived OM, should be reflected in the oceanic organic isotopic composition therefore negative excursion in the ocean's isotopic composition.

2.2 Basinal and facies controls on isotopic composition

Thermodynamic and biological processes have strong opposing influences on the distribution of $\delta^{13}C$ in the ocean surface. Thermodynamic processes, mainly air-sea exchange, influences isotopic fractionation as $\delta^{13}C$ of DIC in isotopic equilibrium with atmosphere is temperature dependant. (Gruber, *et al.,* 1999) About 0,1‰ per degree of cooling, the $\delta^{13}C$ of DIC is higher relative to atmospheric value (Mook, Bommerson, & Staverman, 1974), hence the $\delta^{13}C$ values in warm water are lower than in cold water. Biological processes, result in isotopic effect as phytoplankton takes up lighter isotope ^{12}C over ^{13}C during the photosynthetic fixation of CO_2. The balance between these two influences leads to complex surface distribution pattern but distinct features can still be found in all ocean basins. (Gruber, *et al.,* 1999) Below the photic zone, OM that is depleted in ^{13}C, sinks to lower depths where it remineralizes and lowers overall $\delta^{13}C$ value in the deeper part of the water column, whilst the rejection of ^{13}C by

phytoplanktons in the photic zone increases $\delta^{13}C$ value of surface waters. (Cramer & Jarvis, 2020) These set of processes by which inorganic carbon via photosynthesis is fixed into OM and allocated away from the surface environments into deep ocean is called „biological pump“ (Rocha & Passow, 2014). The magnitude and gradient of biological pump is reliant upon total productivity, organic carbon transport flux from surface to deep and water columns oxygenation state below the photic zone. In the modern oceans water column, $\delta^{13}C$ gradient is approximately 3‰ (Sarmiento & Gruber, 2006), however this value may have been substantially larger during the Proterozoic as present-day oxygenated deep oceans allow less dissolved and particulate organic carbon to reach the deep waters. For Palaeozoic portion of Earth's history, additional care must be taken when interpreting $\delta^{13}C$ data to differentiate truly global signals from potential local overprinting of any given isotopic record. Most of the data from this Era comes from epicontinental carbonates. In these carbonates, absence of unrestricted circulation to the open ocean, increased probability of developing extensive exposure surfaces in time and tendency to include various carbonate minerals with different fractionation coefficients (chapter 2.3), may all impact $\delta^{13}C_{carb}$ values. (Cramer & Jarvis, 2020)

To corroborate the changes in carbonates, the covariance of $\delta^{13}C$ values of inorganic and organic fraction is commonly assessed. Through time this relationship is relatively consistent. However Oehlert, *et al.,* (2012) shows that in shallow marine carbonates there is no correlation between the $\delta^{13}C_{organic}$ and $\delta^{13}C_{inorganic}$ values, but strong covariance can be seen further away from the margin. This is a pseudo-correlation as platform derived materials with relatively positive $\delta^{13}C$ values in organic and inorganic components are mixed with isotopically lighter pelagic material. The correlation breaks down between inorganic and organic fractions closer to the platform, as sediments contain larger proportion of platform material. (Swart, 2015) Although it is not known how applicable these results on relatively recent carbonate sediments are to ancient materials, it is important to consider them when interpreting organic carbon burial, pCO_2 or other fluctuations in the global carbon cycle in shallow marine setting like epeiric seas, platforms and ramps, as bulk records are sourced from a variety of producers in the shallow marine and pelagic environment. (Oehlert, *et al.,* 2012) Difference in carbon isotopic composition along onshore-offshore profile has led to discussion if secular $\delta^{13}C_{carb}$ changes in geological sections have been influenced or caused by changes in depositional setting and/or diagenetic environment changes. In Ordovician carbonate basin, the facies

constrained $\delta^{13}C_{carb}$ bulk-rock values have been recorded in different parts of the world. Specifically, studies from North America and similar studies from Baltoscandian basin show a general lowering trend in $\delta^{13}C_{carb}$ towards the shallower facies. In Hirnantian interval opposite change is documented. (Ainsaar, Meidla, & Hints, 2019)

2.3 Sample scale isotopic heterogeneity of carbonate sediments

It has been shown that $\delta^{18}O$ and $\delta^{13}C$ values in different minerals and components of carbonate sediments that are formed under the same environmental conditions are different. Tarutani, Clayton, & Mayeda, (1969) laboratory experiments show that O isotopes between aragonite, low Mg calcite (LMC) and high Mg calcite (HMC) fractionate differently. $\delta^{18}O$ value of aragonite is usually about 1‰ lower than LMC formed at the same temperature and $\delta^{18}O$ value of HMC compared to LMC increases by about 0.06‰ for every mol% $MgCO_3$. Romanek, Grossmann, & Morse, (1992) laboratory experiments show that carbon isotope erichment factors for aragonite and calcite bicarbonate average 2.7‰ and 1.0‰ accordingly for temperatures 10–40 °C and the resulting fractionation is 1.7‰. This means that $\delta^{13}C$ value of aragonite is typically 1–2‰ higher than co-occurring LMC and HMC. Dolomites formed at 25°C, the same conditions as LMC, have $\delta^{18}O$ values which can be about 3–6‰ heavier. The $\delta^{13}C$ values of dolomite are ca 1‰ higher than LMC but the values are mostly similar to the sediments from which dolomite formed. (Swart, 2015)

One of the processes that can affect the primary signal of isotopic composition of carbonate sediments is diagenesis. Carbonate diagenesis can result in incorporation of ^{12}C from oxidized organic material into pre-existing carbonate minerals that recorded the original $\delta^{13}C$ signature of DIC at the time of their formation causing post-deposition negative shift of bulk-rock $\delta^{13}C$ values. This has particular importance in carbonates collected from outcrops as opposed to drill cores. This is because meteoric waters have a potential to lower $\delta^{13}C$ value of the carbonate and typically will also lower the $\delta^{18}O$ value. (Cramer & Jarvis, 2020) Therefore, positive covariance between $\delta^{13}C$ and $\delta^{18}O$ values is often used to demonstrate the influence of meteoric diagenesis (Allan & Matthews, 1982). Swart & Oehlert, (2018) suggest that covariance between bulk $\delta^{18}O$ and $\delta^{13}C$ values of shallow marine carbonates does not reflect alterations within mixing-zone of the depositional environment, but rather track variable amounts of recrystallization/neomorphism and the addition of diagenetic

cement. Also, the lack of covariance in marine carbonates does not necessarily prove that the material maintains its original signal. Carbonate rocks that have been pervasively altered in the vadose zone often do not have covarying trend and in some instances where strong covariance in unaltered carbonate material can be found, mixing of material with different isotopic composition is found. Remineralization of organic carbon under diagenesis, is another mechanism that can introduce ^{12}C during cementation and/or diagenetic stabilization which lowers the $\delta^{13}C$ value (Cramer & Jarvis, 2020).

Because of diagenetic processes, fossils and micro fossils of LMC are preferred for stable isotope stratigraphy over aragonite and HMC, as LMC is more resistant to diagenesis and therefore original signal persists longer in sedimentary record. Shell size and texture also factor in preservation as thick and dense shells retain original isotopic composition better than thin and more porous shells. This is why brachiopod shells are typically 2–3‰ higher in $\delta^{18}O$ value compared to encasing diagenetically modified bulk carbonate. (Grossman & Joachimski, 2020) Similar $\delta^{13}C$ contrast between the bulk-rock and brachiopods is shown by Hints, *et al.,* (2010) in the Ordovician Porkuni Stage of Stirnas-18 core representing one of the most complete Hirnantian succesion in the eastern Baltic region. $\delta^{13}C$ values derived from brachiopod shells are about 2‰ more positive in $\delta^{13}C$ value compared to bulk-rock values. Gul, *et al.,* (2021) also show that in the Ordovician-early Silurian interval of the Baltoscandian Palaeobasin the $\delta^{13}C$ and $\delta^{18}O$ values tend to be more positive in brachiopods compared to bulk-rock. Differences in isotopic composition in different organisms can also be produced by "vital effect". Metabolic CO_2 from sources like food and respiration play a role on skeletal isotopic composition of organisms and this may also apply to organisms that do not have symbiotic algae. Vital effect should be accounted for in palaeoenvironmental reconstructions based on stable-isotope composition of biogenic carbonates (Erez, 1978).

3. Hirnantian Isotope Carbon Excursion and Mid-Ludfordian Carbon Isotope Excursion

During Middle to Late Ordovician, major perturbations in the global carbon cycle were widespread. There are many locally named CIEs that are not recognized between basins and in addition to local processes affecting $\delta^{13}C_{carb}$ values, significant isotopic heterogeneity can be observed within single hand sample. Hirnantian Isotope Carbon Excursion however is one of the best documented CIEs from multiple basins/continents with a magnitude of ∼8‰ (Goldman, *et al.,* 2020). Litho- and chemostratigraphic evidence shows clearly that the peak glacial expansion of the Ordovician-Silurian took place in early-mid-Hirnantian. In addition of suggested global cooling by oxygen isotopic data, spreading of glacial and glaciomarine sediments in Hirnantian time and the palaeogeographic distribution of benthic fauna indicates that cool-water faunas may have migrated into lower palaeo-altitudes supporting overall global cooling. This means that HICE directly reflects the climatic change. (Melchin, *et al.,* 2013)

Carbon isotope ratios measured from carbonates dated to Silurian period, shows that Silurian seawater was highly variable through time. This indicates that the global carbon cycle and global climate system were less stable in Silurian period compared to other periods during Phanerozoic. The most pronounced positive excursion of the seawater $\delta^{13}C$ occurred during middle Ludfordian, representing the largest post-Cambrian $\delta^{13}C_{carb}$ excursion of the entire Phanerozoic. (Melchin, Sadler, & Cramer, 2020) This excursion with magnitude of ∼9‰ is named Mid-Ludfordian Carbon Isotope Excursion (MLCIE) accompanied with “Lau event” which was stepwise extinctions of conodont species that was first recognized in the carbonate platform succession of Gotland. Thus far causes for Silurian CIEs are not fully understood. Climate change, glaciation, sea-level changes, enhanced primary productivity, increased marine anoxia, ocean circulation and variations in Earth’s solar insolation induced by orbital changes in general are some of the conceptual models proposed to explain these excursions. (Frýda, *et al.,* 2021) Testing these models is problematic and main reason for this is general lack of combined high-resolution geochemical/isotope data, biostratigraphic records, detailed sedimentological and palaeontological records from the same sections. This is why concept of High-Resolution Event Stratigraphy (HiRES) is now being applied to Palaeozoic (Cramer, Vandenbroucke, & Ludvigson, 2015).

4. Geological setting

Studied samples in this thesis are collected from drill cores of Ordovician and Silurian strata of the late Ediacaran and Palaeozoic Baltic Basin (BB) in Estonia and Lithuania respectively (Figure 1). The BB is part of marginal basins system, situated along the western edge of the East European Craton (EEC). It includes Peri-Baltic sub-basin that is located near present-day Baltic Sea and Peri-Tornquist sub-basin along the Tornquist-Teisseyre Zone (TTZ) which forms the southwestern margin of the basin. Mazury-Belarus High is situated along southeastern margin of the BB and Fennoscandian Shield lies to the north and north-east. (Lazauskiene, *et al.,* 2002). The Early Palaeozoic sea covering BB in the eastern Baltic and large areas on the Fennoscandian Shield in the west has been described as epicontinental Baltoscandian Palaeobasin (Jaanusson, 1973).

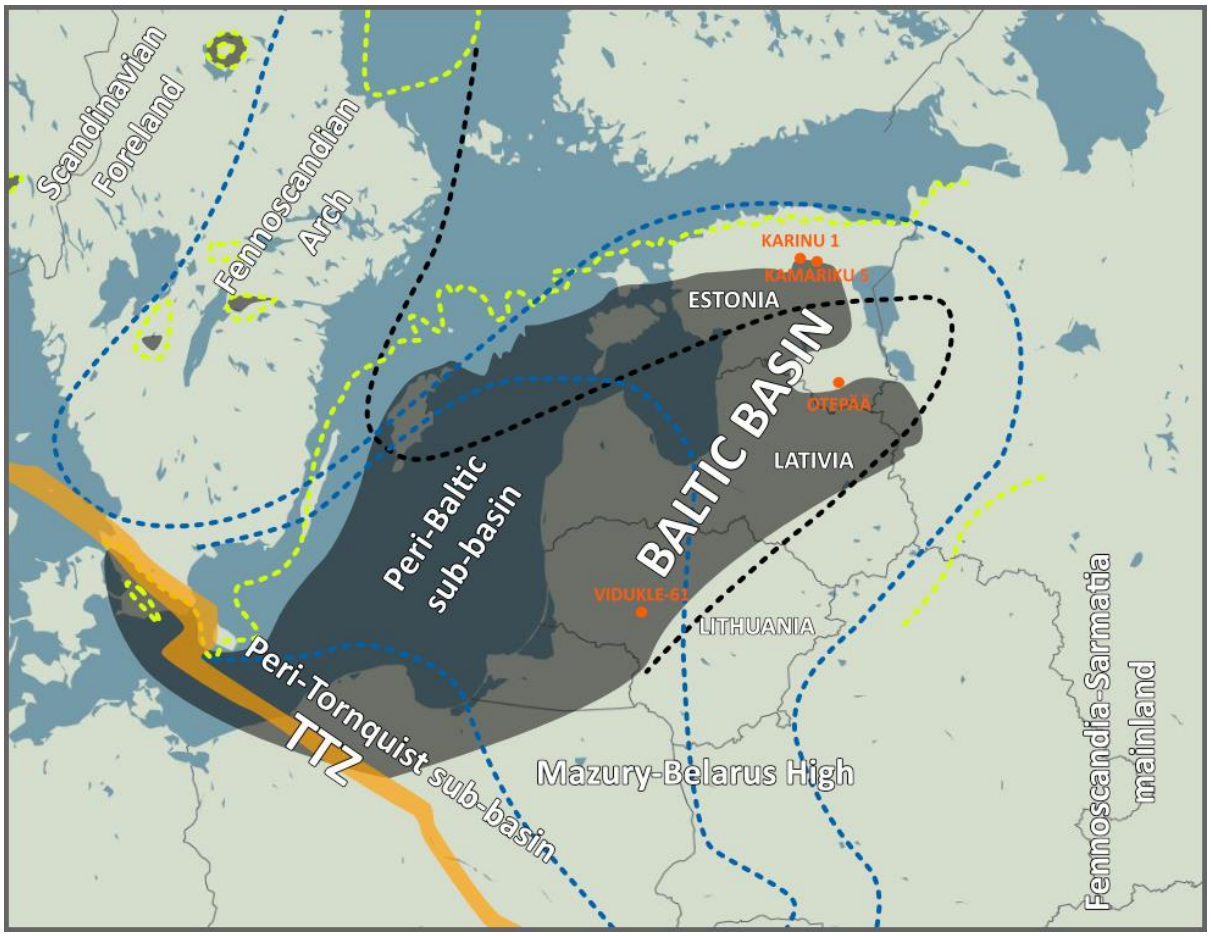

Figure 1. Geological setting of the Baltic Basin (BB) and locations of studied boreholes marked in red circle. Orange area represents Tornquist-Teisseyre Zone (TTZ). Dark grey area represents distribution of Silurian and green dashed line Ordovician sediments in the BB. Black dashed

line shows the boundary between the major Late Ordovician facies belts. Blue dashed line gives an indication of original shape of the BB (from facies trends). (Modified from Ainsaar, Truumees, & Meidla, (2015); Lazauskiene, et al., (2002))

The sedimentary succession of BB includes late Ediacaran and all Palaeozoic strata which experienced rather persistent subsidence. Close to the TTZ the thickness of sedimentary succession reaches more than 5 km and about 75% of the basin fill is comprised of Palaeozoic sediments, with Silurian strata being dominant and most complete succession of the BB. Silurian succession overlies 80–220 m thick Ordovician succession with stratigraphic break, indicating regional regression and shallowing of the sedimentary basin at the end of the Ordovician. (Lazauskiene, *et al.,* 2002)

During the Hirnantian, the Baltica palaeocontinent was situated at relatively low southern latitudes drifting northwards and reaching equator during early Silurian. Shallow water depositional settings developed during Ordovician in the location of present-day Estonia, eastern part of the BB and western part of Baltica palaeocontinent (Figure 2). (Cocks & Torsvik, 2005) Ordovician period had most extensive distribution of epicontinental seas experiencing accumulation of ubiquitous carbonate sediments. During Ordovician, marine flora and fauna changed considerably and number of major taxonomic groups either appeared or became common. In respect of marine fauna, Estonia has one of the best preserved fossil records. Estonian Ordovician succession ranges from 70–180 m in thickness. (Nõlvak, 1997) In this thesis, studied Ordovician samples were taken from the succession recording HICE in the Porkuni Stage (Figure 3). Porkuni Stage is the topmost Ordovician stage and is represented by lithologically variable deposits of shallow-water facies, with thickness of about 10 m in northern and up to 18 m in southern Estonia. The Ärina Formation represents the Porkuni Stage in northern Estonia and comprises a succession of dolomites (Röa Mb.), skeletal limestones (Vohilaid Mb.), limestones with bituminous interlayers (Siuge Mb.), stromatoporoid-tabulate reefs and oolitic or sandy limestones (Kamariku Mb.) in the top. Peripheral parts of the Saldus Formation represent the topmost part of the Porkuni stage in southern Estonia and comprises of silty and sandy limestones with lithoclasts and carbonate ooids. (Hints & Meidla, 1997)

During the late Wenlock and Ludlow time, Silurian sediments that are now located in present-day Lithuania, were deposited in the eastern part of the BB in the equatorial setting (Figure

2) (Cocks & Torsvik, 2005). Silurian open marine environments were represented in western part and shallow marine environments in the eastern part of Lithuania. The sections in the western part of the Lithuanian are considered to represent the most complete sedimentary succession of late Wenlock and Ludlow. The investigated interval includes the Dubysa and Pagegiai regional stages, both representing the Ludfordian Stage. The Mituva Formation of the Pagegiai Stage is composed of argillaceous limestone in the lower part and undulated limestone in the upper part and includes the MLCIE interval. (Spiridonov, *et al.,* 2020)

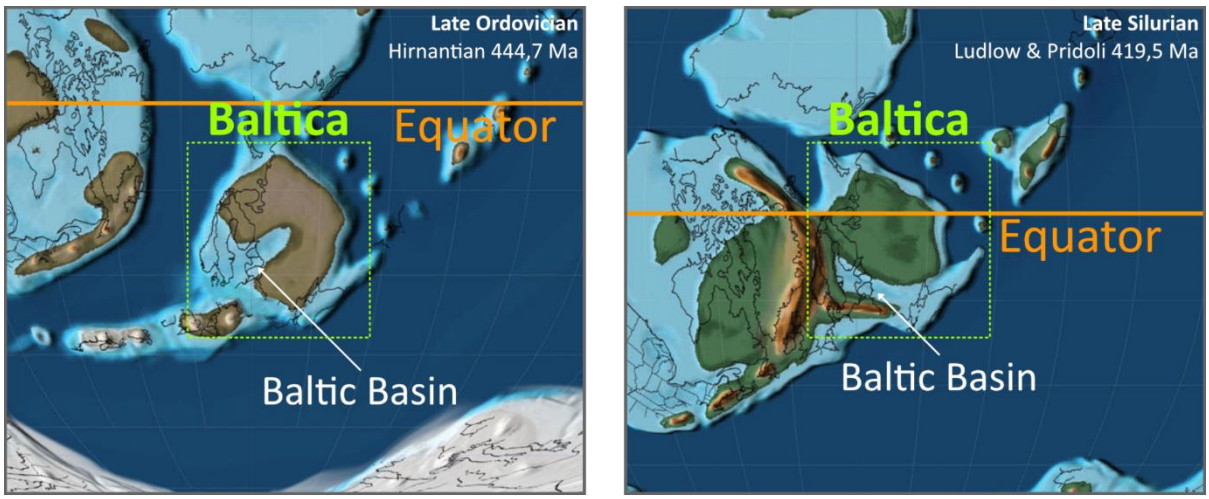

Figure 2. Palaeogeogrpahic maps of Late Ordovician and Late Silurian showing the drift of the Baltica continent towrds equator. (Modified from Scotese, (2014))

5. Materials and methods

Carbonate rock samples representing HICE and Lau MLCIE were collected from cores drilled in Estonia and Lithuania (Figure 1). The selection of samples was guided by lithology and previous isotope data recording above-mentioned CIEs as shown in Figure 3. Altogether 6 rock samples were collected. For HICE, four intervals from Kamariku 5, Karinu 1 (Ainsaar, Truumees, & Meidla, 2015) and Otepää drill cores (Oraspõld, 1975) representing the Porkuni stage were chosen. From Kamariku 5 drill core, two rock samples (K5-1 and K5-2) were taken from depths 17.38 m (Kamariku Mb) and 19.2 m (Siuge Mb) accordingly. From Karinu 1, one rock sample (K1) from depth 33.52 m (Vohilaid Mb). From Otepää section one rock sample (OP) originally collected by Asta Oraspõld from depth 374.6 m (Saldus Formation; Table 10, Figure 2 in Oraspõld, (1975)) was studied. For MLCIE, samples from the Vidukle 61 drill core were chosen to describe Ludfordian Stage. Two rock samples (VID1 and VID3) are from depths 1142.5 m (Sample from the collection of Taltech, Institute of Geology; Martma, Sample No. 185844, (2022)) and 1147.6 m (Sample from the collection of Taltech, Institute of Geology; Martma, Sample No. 185848, (2022)) (Mituva Fm) accordingly (Martma, *et al.,* 2005).

Polished thin sections (100 µm thickness) of all samples were prepared at Independent Petrographic Service Ltd in Scotland. Thin sections were petrographically studied and imaged using LEICA M205 A optical microscope (Figure 4; Figure 5). Elemental mapping of polished thin sections was performed with a M4 Tornado µ-XRF instrument from Bruker at the Norwegian University of Science and Technology (NTNU), Trondheim. Polished thin sections were placed together into the µ-XRF, for simultaneous elemental mapping. These maps were used for an overview of dolomite and calcite relationships in samples and trace element variations among individual components. The instrument operates with an Ag X-Ray source and two silicon drift detectors simultaneously for fast analysis. A collimator focuses the X-ray beam to a spot size of about 20 µm. Elemental maps including major elements Al, Ca, Fe, K, Mg, Mn, S, Si and Ti were acquired with 50 kV accelerating voltage and 600 µA tube current. A distance of 20 µm between each measuring point and a speed of 4 ms/pixel were chosen for qualitative maps. For each map, the signal detected as counts per second (cps) is normalized to 100 %. The brightest areas represent the highest measured cps. The total scan time was about 25 hours. Measurements were performed under vacuum at 20 mbar.

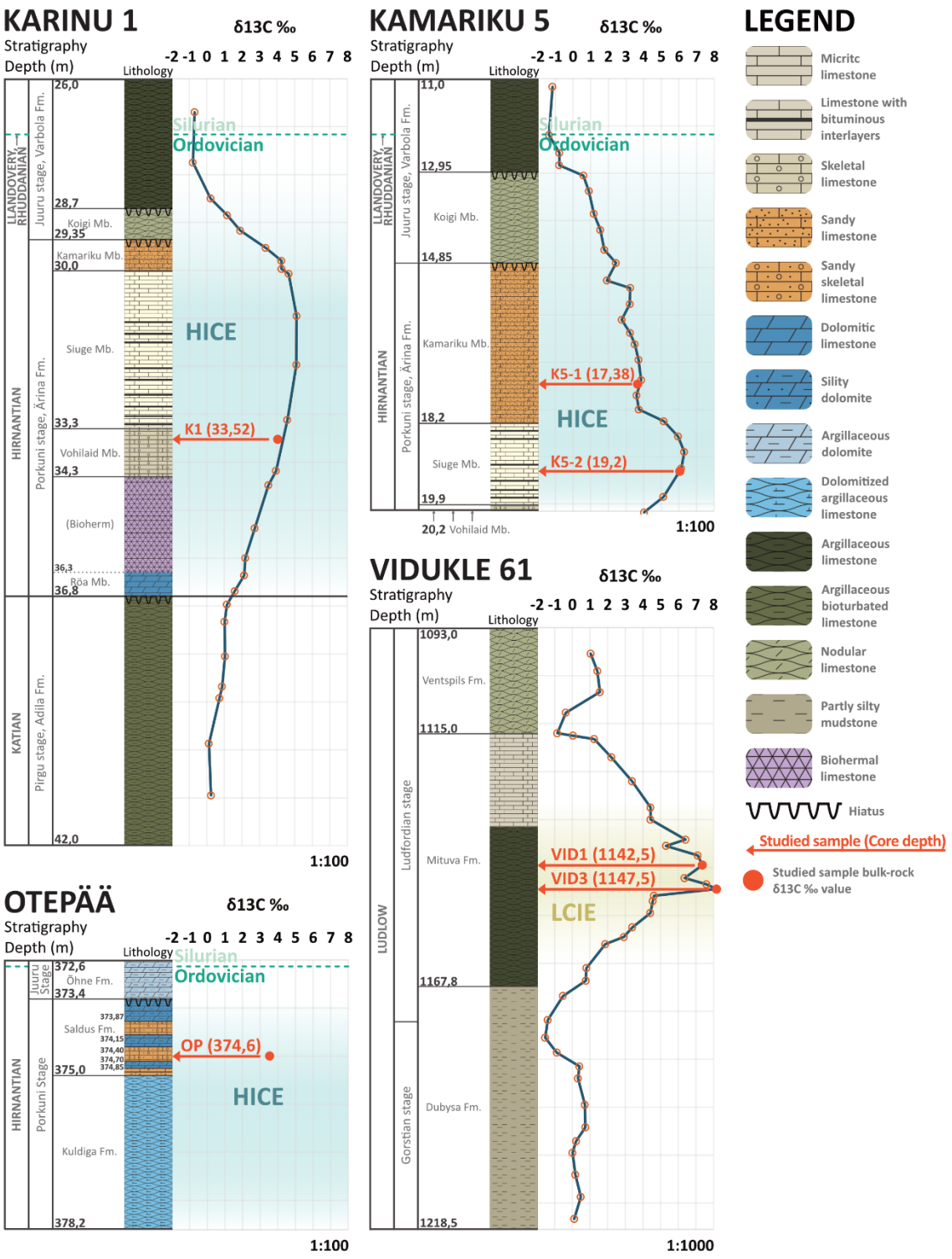

Figure 3. Stratigraphy, previously published δ13C curves and positions of studied samples in targeted drill cores. Karinu 1 and Kamariku 5 by (Truumees, 2012), Otepää by (Oraspõld, 1975) and Vidukle 61 (Martma, et al., 2005). (All figures modified)

Thin section offcuts of four HICE samples were used for micro-drilling of rock powders from different rock components. Isotopic analysis of bulk-rock and micro-drilled sub-samples were done by isotope-ratio mass-spectroscopy (IRMS) using Delta V Advantage mass-spectrometer with Gas-Bench II interface (manufactured by Thermo Fisher Scientific) at University of Tartu. Samples were dissolved in phosphoric acid (H_3PO_4, 99%) with reaction time of >8 hours. Data was calibrated against following international standards from IAEA: NBS 18 ($\delta^{13}C_{carb}$ = -5.029‰; $\delta^{18}O_{carb}$ = -23.2‰), IAEA 603 ($\delta^{13}C_{carb}$ = 2.46‰; $\delta^{18}O_{carb}$ = -2.37‰), LSVEC ($\delta^{13}C_{carb}$ = -46.6‰; $\delta^{18}O_{carb}$ = -26.7‰), IAEA 611 ($\delta^{13}C_{carb}$ = -30.795‰). Standard deviation of the data is σ=0,05‰ and the results are reported respective to V-PDB standard. For preparing thin sections, rock samples were impregnated with epoxy and therefore some micro-drilled sub-samples from offcuts contained epoxy powder. Epoxy, if presented, gives micro-drilled powders a bluish colour but it does not affect carbonate isotope results. Epoxy does not react with H_3PO_4; one pure epoxy powder was analysed with no signal detected.

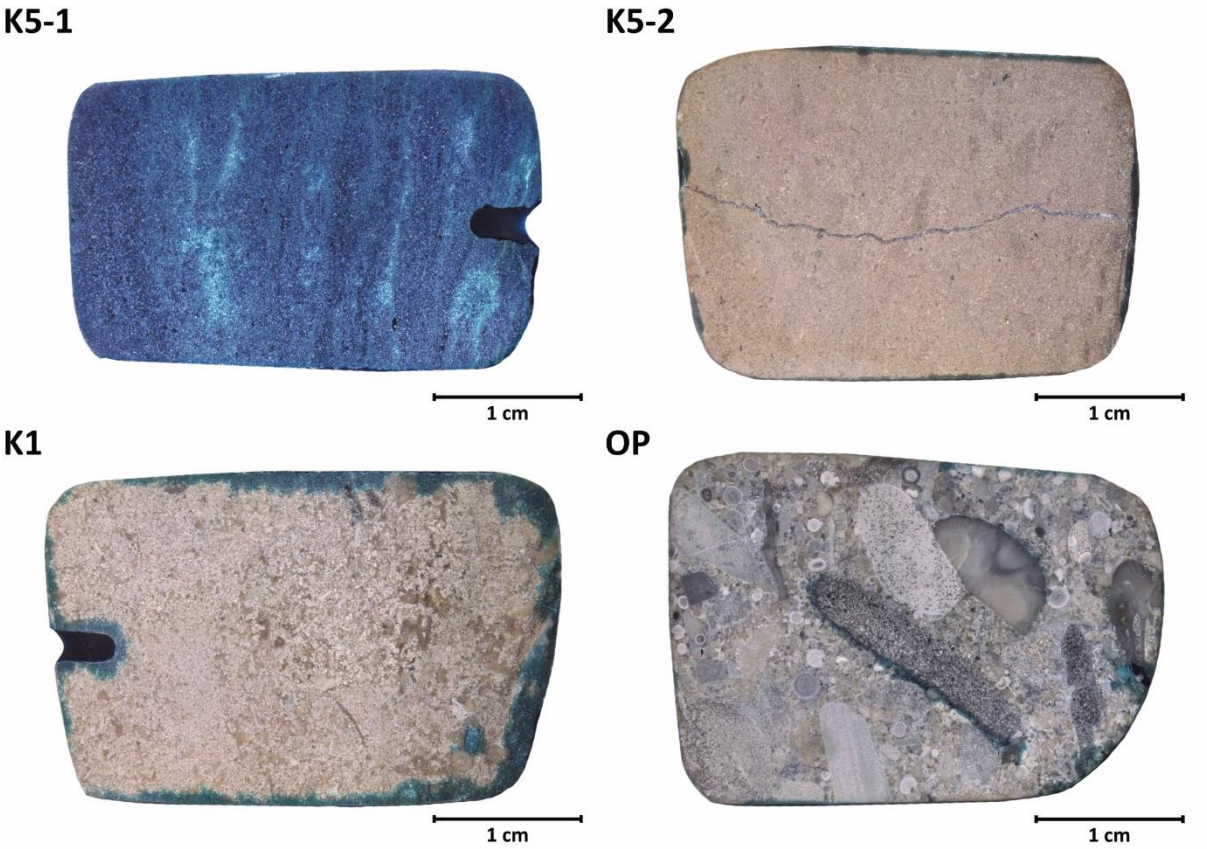

Figure 4. Images of epoxy impregnated thin section offcuts.

Altogether 45 sub-samples were carefully micro-drilled from different rock components and one bulk-rock sample from each rock was taken. For micro-drilling, 0.7 mm and 1.8 mm diamond drill bits were used, depending on rock component dimensions and the aluminium foil was placed on the drilling stand to collect powder. Approximately 0.1–0.3 mg of powder was drilled and weighed depending on components dolomite and silica content. Drill bits were first cleaned with fiberglass brush and both drill bit and aluminium foil were subsequently cleaned with ethanol and dried with compressed air after every micro-drilled sub-sample.

Lithologically and isotopically most heterogeneous OP sample was chosen for determining elemental concentrations in components. Three to four laser ablation inductively coupled plasma mass spectrometry (LA-ICP-MS) spot measurements were made close to every micro-drilled location and these measurements were taken from visually different parts around the micro-drilled location to get average elemental concentrations of the studied component. The LA-ICP-MS measurements were performed in University of Tartu, using an Agilent 8800 quadrupole ICP-MS coupled to a Cetac LSX- 213 G2+ laser with HelEx II fast-washout two-volume large-format cell and 'Squid' smoothing interface. Spot analysis on the samples was performed using the following laser parameters: fluence 3.2J/cm2, repetition rate 10 Hz, 50µm round spot. 20s of gas blank were collected before each ablation pass and ablation signal was collected for 50s. USGS GSD1G was used as primary calibration standard and KCSp1 NP (nano pellet) from GProbe proficiency testing scheme was used as a secondary standard. Oxide formation ratio expressed as ThO/Th from ablation of NIST 610 during instrument tuning was <0.25%. Signals of 24Mg, 27Al, 29Si, 31P, 43Ca were collected with a dwell time of 6 ms, 88Sr with a dwell time of 6.7ms and 55Mn, 57Fe, 89Y, 137Ba, 139La, 140Ce, 141Pr, 146Nd, 147Sm, 153Eu, 157Gd, 165Ho, 206Pb and 238U were collected with a dwell time of 7 ms, surmounting to a total duty cycle of 0.2s on the ICP-MS. Data reduction of the raw signals were performed using Iolite V3.62. After background substitution signals were normalised to GSD1G using X_Trace_Elements_IS data reduction scheme with quantitative standardisation method using Ca as internal standard element. For samples, a stoichiometric calcite Ca concentration of 40.04 wt% was used assumed.

Thin section offcuts of two MLCIE rock samples were chosen for in-situ isotope analyses by secondary ion mass spectrometry (SIMS). In situ analyses of $^{18}O/^{16}O$ and $^{13}C/^{12}C$ ratios were

conducted using the CAMECA 1280-HR large geometry SIMS instrument at the Helmholtz Centre Potsdam – GFZ German Research Centre for Geosciences. The rock fragments representing ~15 mm discs cut from thin section offcuts were mounted in epoxy resin in the centre of two 25.4 mm diameter acrylic discs, which were subsequently polished. Prior to analyses the sample mounts were cleaned in high-purity ethanol ultrasonic bath and coated with a 35 nm thick, high-purity gold film to assure electrical conductivity during analyses. The measurements were conducted in four fully automatic, chain-analysis sequences in February and April 2022. A nominally 2 nA, 10 keV $^{133}Cs^{+}$ primary ion beam was focused to a 10 µm diameter spot on the sample surface. A normal incidence electron gun was used for charge compensation.

Oxygen isotope analysis was carried out, using a rastered beam, a 25 µm × 25 µm area of the sample surface was pre-sputtered for 70 seconds to remove the gold coat, suppress surface contaminants and establish equilibrium sputtering conditions. The raster was then reduced to a 15 × 15 µm area to ensure a flat-bottom crater geometry, from which $^{18}O^{-}$, $^{16}O1H^{-}$, and $^{16}O^{-}$ secondary ions were collected simultaneously on three Faraday cups, over 20 cycles with each cycle lasting for 4 seconds. A typical count rate for $^{16}O^{-}$ ions was ~1.3 x 10^{9} cps. The mass resolution of the instrument was set to M/ΔM ≈ 4700 (at 10 % peak height) in order to resolve the $^{16}O^{1}H^{-}$ and $^{17}O^{-}$ peaks. Carbon isotope analysis was carried out, using a 20 × 20 µm raster, the sample surface was pre-sputtered for 75 seconds. The raster was then reduced to a 15 × 15 µm area, from which $^{13}C^{-}$ and $^{12}C^{-}$ secondary ions were collected simultaneously on two Faraday cups, over 40 cycles with each cycle lasting for 4 seconds. A typical count rate for $^{12}C^{-}$ ions was ~2.3 x 10^{7} cps. The FC2 Faraday cup on which $13C^{-}$ was collected is equipped with a 10^{12} Ω amplifier. The mass resolution of the instrument was M/ΔM ≈ 3200 (at 10 % peak height).

Data reduction for the measured $^{18}O/^{16}O$ and $^{13}C/^{12}C$ ratios were corrected for instrumental mass fractionation (IMF) based on the calcite reference material UWC-3 that was mounted in the centre of each acrylic disc and whose analyses were regularly interspersed throughout the runs. The $\delta^{18}O_{VSMOW}$ of UWC-3 is 12.49 ± 0.03‰ (1s) and the $\delta^{13}C_{PDB}$ is -0.91 ± 0.04‰ (1s; Kozdon, et al, 2009). No drift was observed throughout the analytical sessions devoted to oxygen isotopes, and the repeatability of the $^{18}O/^{16}O$ measurements conducted on UWC-3 was ± 0.2‰ (1s). During carbon isotope measurements, instrumental drift was observed and,

therefore, the $^{13}C/^{12}C$ data were corrected based on the analyses done in UWC-3 grains; the repeatability of $^{13}C/^{12}C$ determinations was ± 0.6‰ (1s). Consequently, we estimate that the quality of our data is better than 0.2‰ (1SE) for oxygen and 0.6‰ (1SE) for carbon. Oxygen and carbon isotope ratios in the investigated samples are expressed relative to the Vienna Pee Dee Belemnite (V-PDB, $^{13}C/^{12}C$ = 0.0112372; Craig, (1957); Allison, Francey, & Meijer, (1995)). Measured oxygen isotope ratios were first expressed relative to the Vienna Standard Mean Ocean Water ($^{18}O/^{16}O$ = 0.0020052; Baertschi, (1976)) and then converted to V-PDB using equation (32) in Brand, *et al.,* (2014).

Prior SIMS analysis, detailed image documentation was prepared for optimal placement of 20 µm analysis spots. This documentation included optical (OPT), reflected-light (RL) and backscattered electron (BSE) imaging (Figure 5). Optical and BSE images, combined with XRF-mapping information allowed best identification of different components and inclusion free areas. RL images were used to select analysis spots on morphologically smooth areas and for defining the analyses chains in the SIMS instrument. Although OPT, RL and BSE images were aligned as best as possible, some areas are lightly misaligned. Example can be seen on VID-1 sample, area 9 on Figure 6. SIMS analyses were carried out within predefined 1x1 mm (10 spots) or 1x2 mm (20 spots) areas. Eleven such areas were defined for VID-1 and five areas for VID-3. Optical images of all these areas and placement of SIMS spots are shown on Figures 22 and 23. Altogether 200 SIMS spot measurements were made during two consecutive analytical sessions. In the first session O isotopic composition was measured and in the second session C isotopic composition was measured in spots adjacent (~30 µm shifted) to O spots. These adjacent analyses are considered as coupled C and O measurements. Many of the spot measurements had to be rejected (Figure 7) due to cracks and/or uneven nature of spots and presence of impurities and inclusions. All spots were inspected under microscope after SIMS analysis, and the ones containing clear inclusions were assigned "rejected" status and the ones containing possible inclusions were assigned "warning" status (Table 2; Table 3). The relative secondary ion yields were also examined and spots with yields outside of the value 1.0 ± 5% relative to standard were rejected. After evaluation of $\delta^{13}C$ and $\delta^{18}O$ data separately, all the combined data were divided into six quality status categories (Figure 7). Assuming that small cracks and inclusions have limited effect on obtained isotope ratios, the data carrying "warning" status are used but care is taken when interpreting these data points.

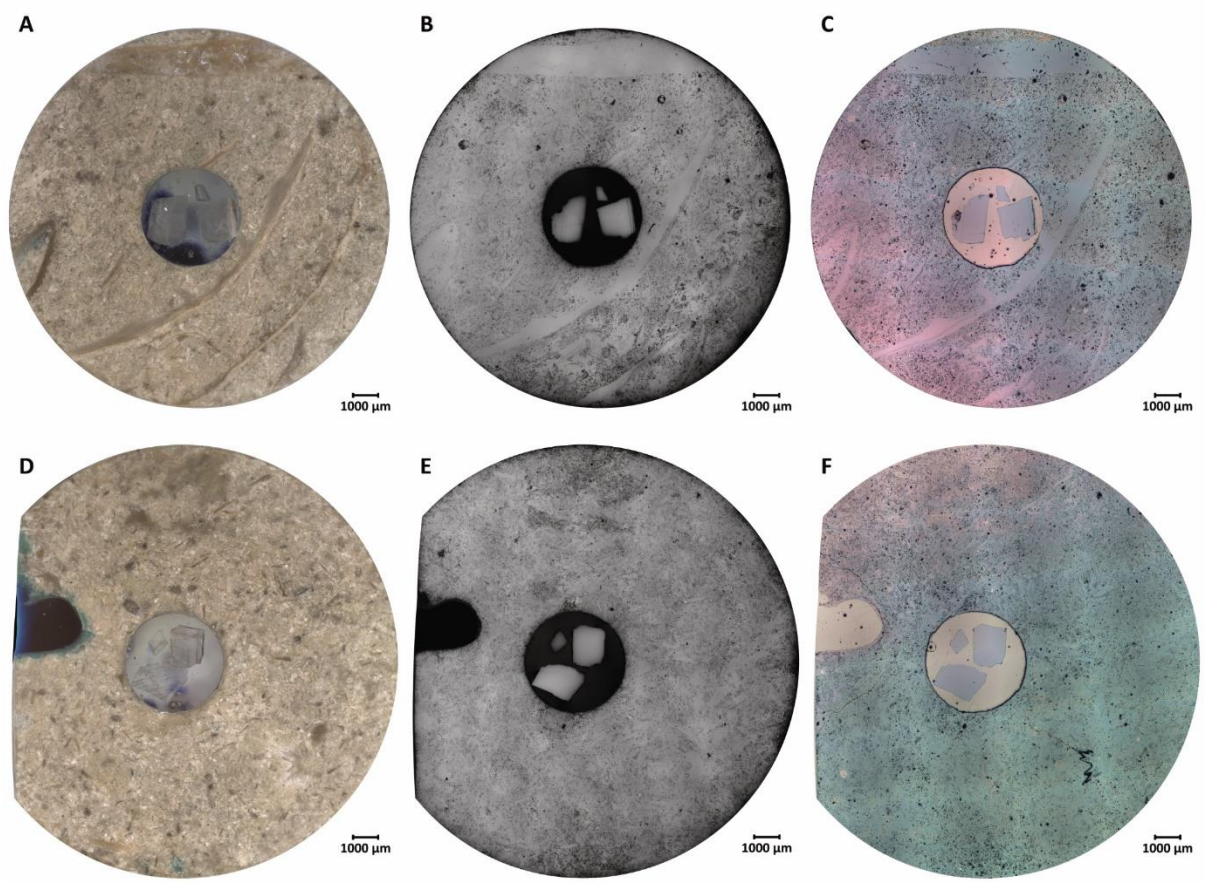

Figure 5. Imaging documentation of SIMS samples VID-1 and VID-3. Panels A, B and C represent OP, BSE and RL images respectively of VID-1 sample. Panels D, E and F represent OP, BSE and RL images respectively of VID-3 sample. Pink and bluish coloration on RL images is caused by gold coating.

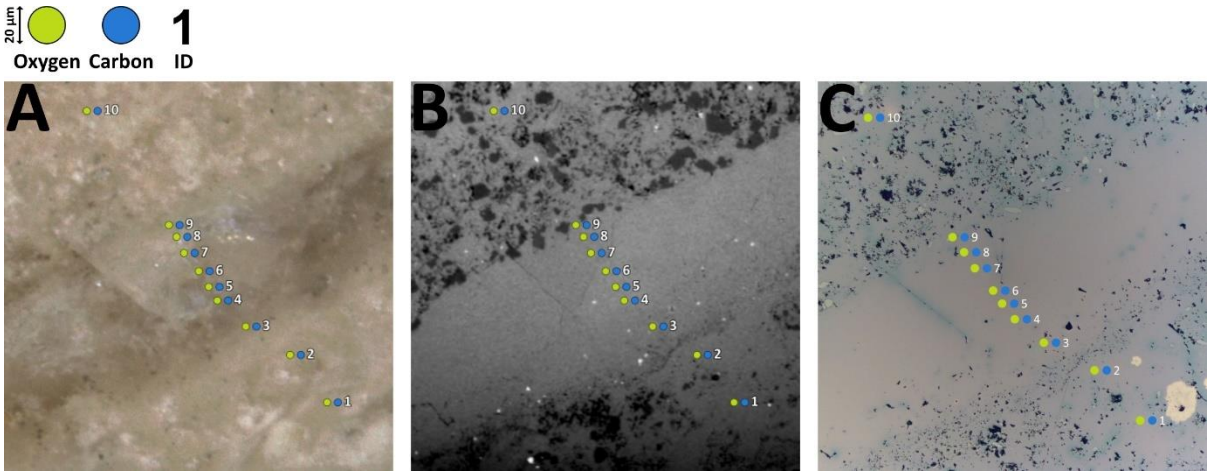

Figure 6. Area 9 in studied sample VID-1 with selected SIMS measurement spots for oxygen (green) and carbon (blue) isotopes. A, B and C are OPT, BSE and RL images respectively.

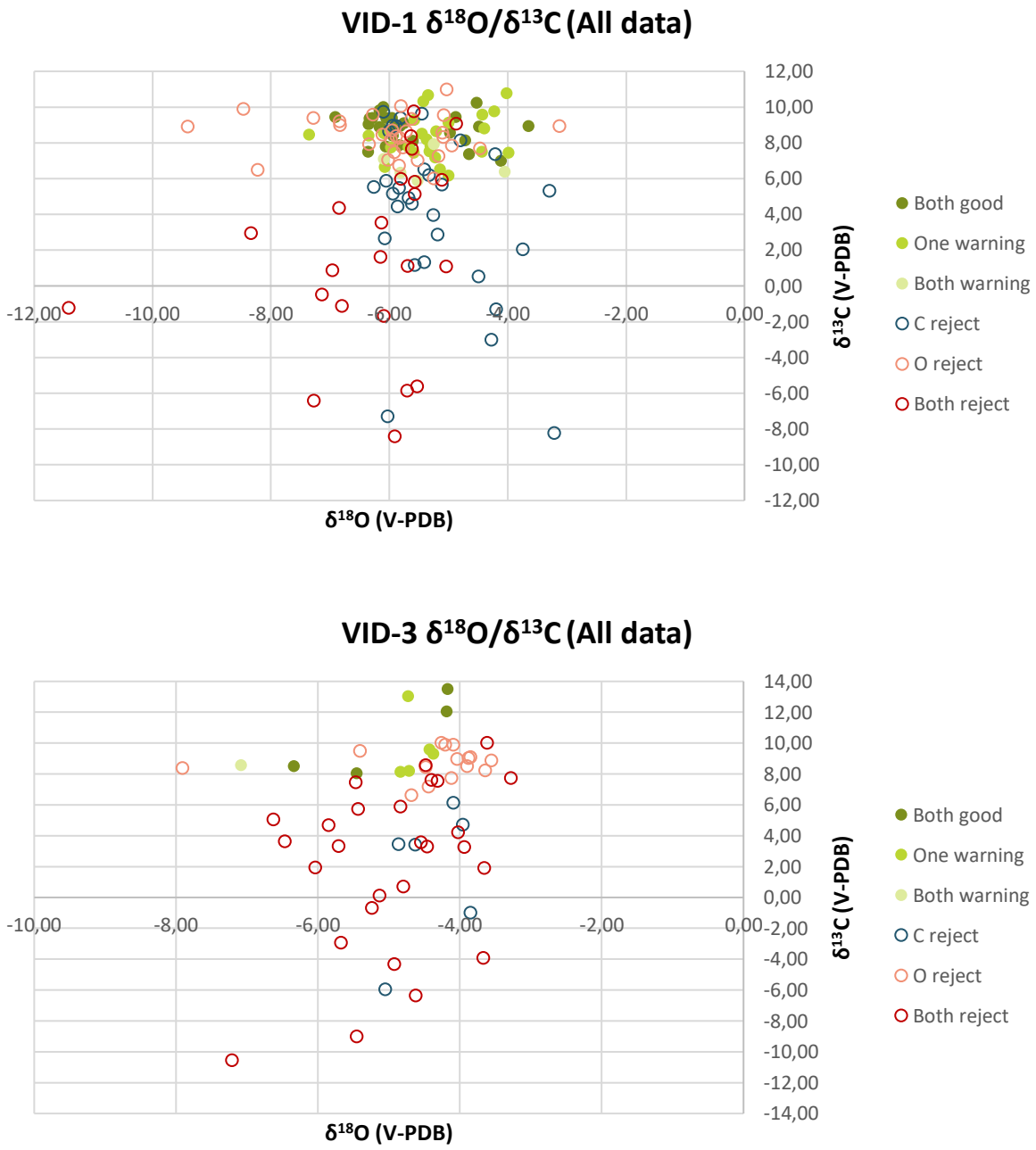

Figure 7. All data for studied samples VID-1 and VID-3 labelled based on quality status.

Reflected-light optical images were taken using Motorized Optical Microscope: Nikon Eclipse before and after gold coating. Backscattered images were taken before gold coating in University of Tartu using scanning electron microscope (SEM) ZEISS EVO MA15 SEM in backscattered electron mode under low vacuum, therefore no sample coating was needed.

6. Results

Isotopic analysis of micro-drilled samples was performed on different components, to assess sample-scale variability during $\delta^{13}C$ excursions. For all samples positions of micro-drilling are shown on optical images and isotope data are presented as $\delta^{18}O$ vs $\delta^{13}C$ cross-plots. The µ-XRF mapping results of Ca and Mg are presented for all samples (Figure 8). For Ordovician samples, additional elemental data are presented to assess if there are any correlations between isotopic composition and elemental concentrations.

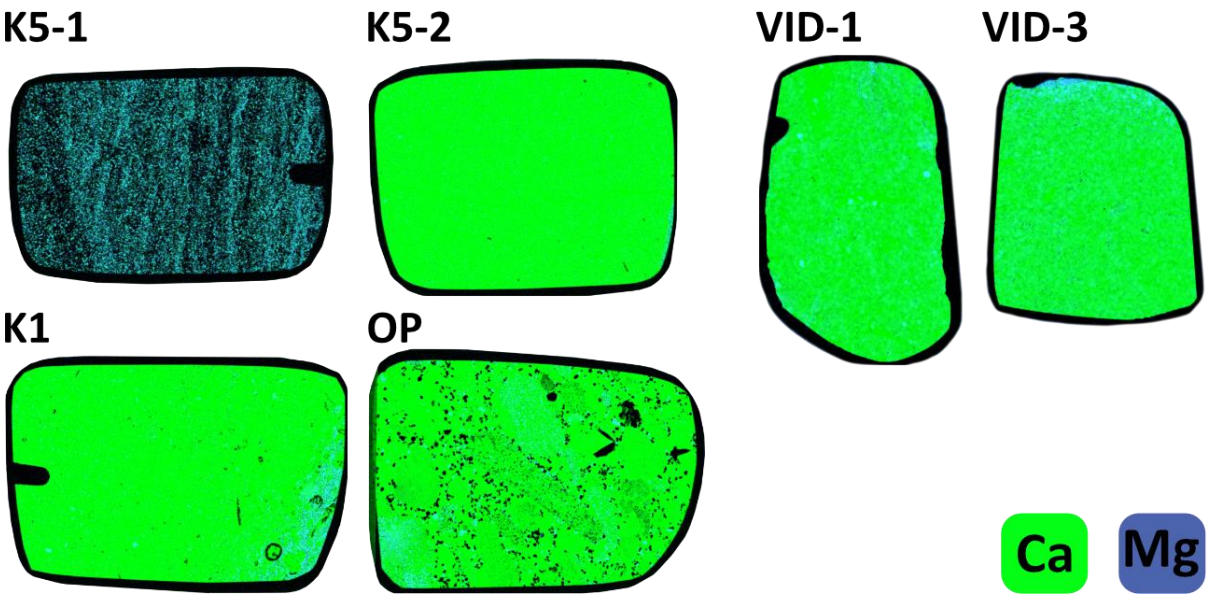

Figure 8. Combined µ-XRF Ca and Mg elemental maps of thin sections for all studied samples. The brightest areas represent the highest measured cps. All samples are calcite dominated (green colours) except K5-1 which contains dolomite (blue colours) as main carbonate phase.

Sample K5-1 is diffusely laminated dolomitic sandstone. Micro-drilling was undertaken in visually different parts of the sample including lighter (higher dolomite, more Mg) and darker (lower dolomite, less Mg) laminae (Figure 9; Figure 9). As shown on the graph (Figure 10), $\delta^{13}C$ is less variable (~0.5‰) between different sub-samples compared to $\delta^{18}O$ (~2‰) and bulk-rock $\delta^{18}O$ and $\delta^{13}C$ values are heavier than values obtained from micro-drilled sub-samples.

K5-1

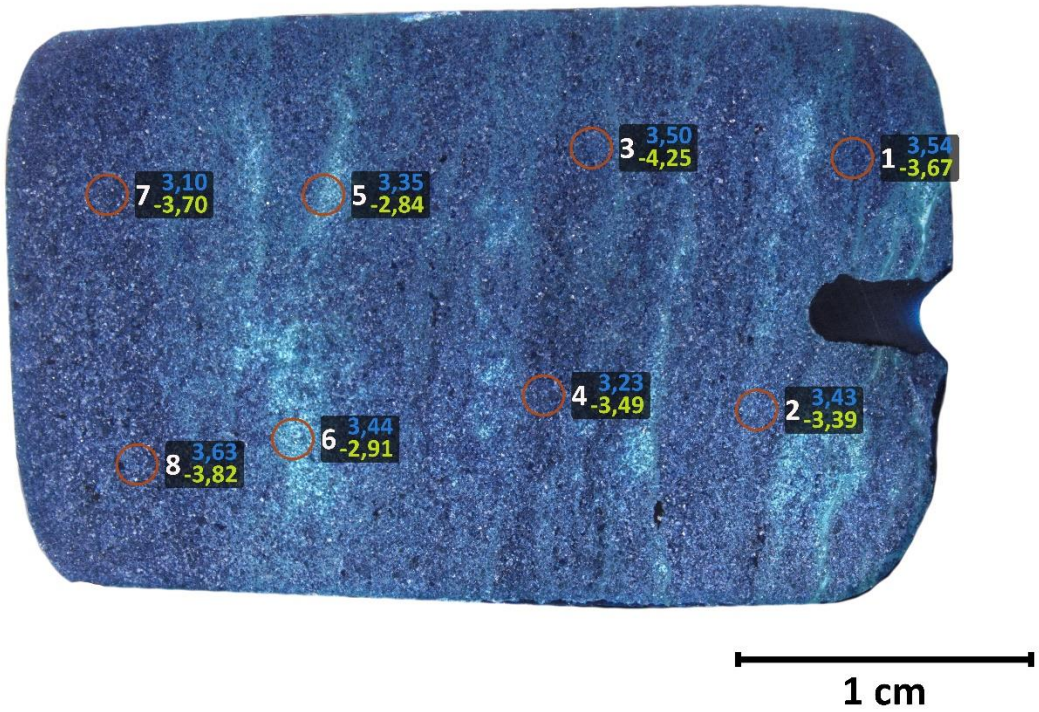

Figure 9. Optical image of K5-1 sample. Red circles correspond to micro-drilling spots and dark boxes list corresponding sample numbers (white), $\delta^{13}C$ values (blue), $\delta^{18}O$ values (green).

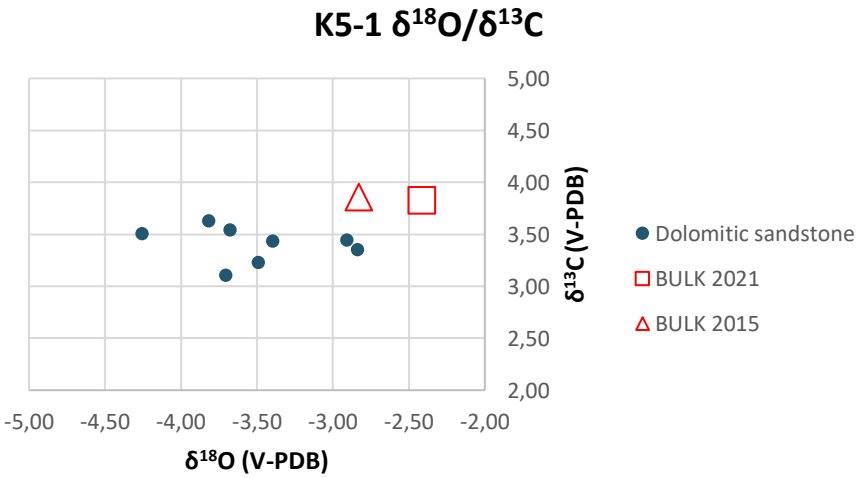

Figure 10. Cross-plot of $\delta^{18}O$ and $\delta^{13}C$ value for K5-1. Results on micro-drilled samples are compared to previous bulk-rock data.

K5-2

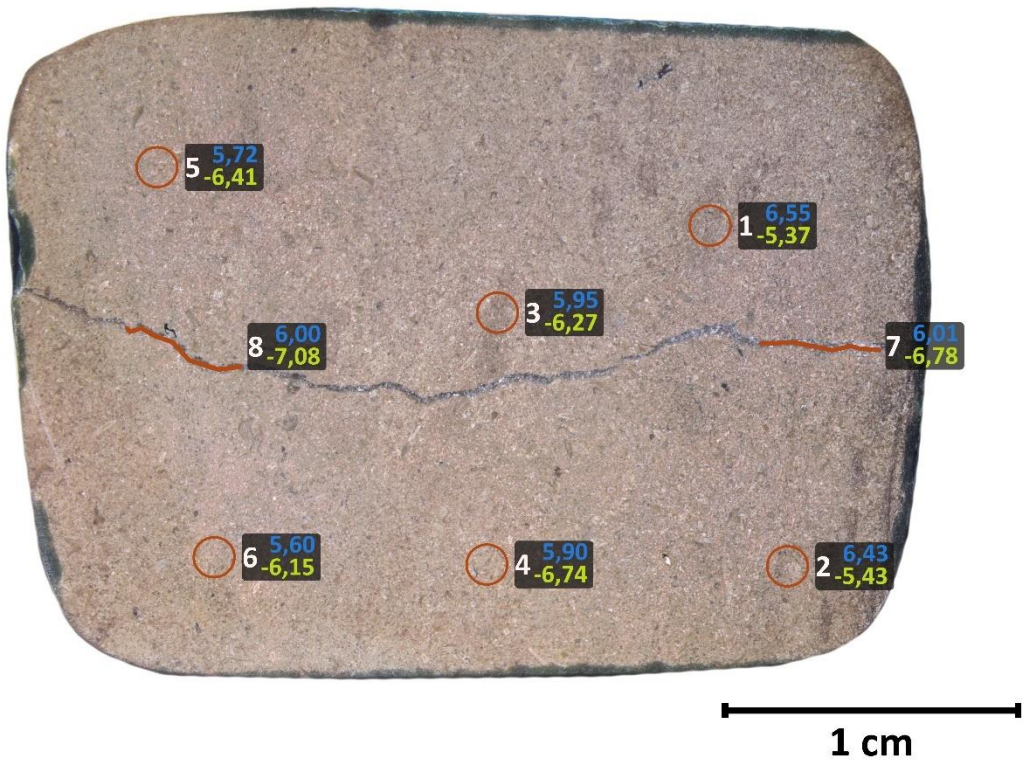

Figure 11. Optical image of K5-2 sample. Red circles correspond to micro-drilling spots, red lines to parts where calcite vein was micro-drilled and dark boxes list sample numbers (white), $\delta^{13}C$ values (blue), $\delta^{18}O$ values (green).

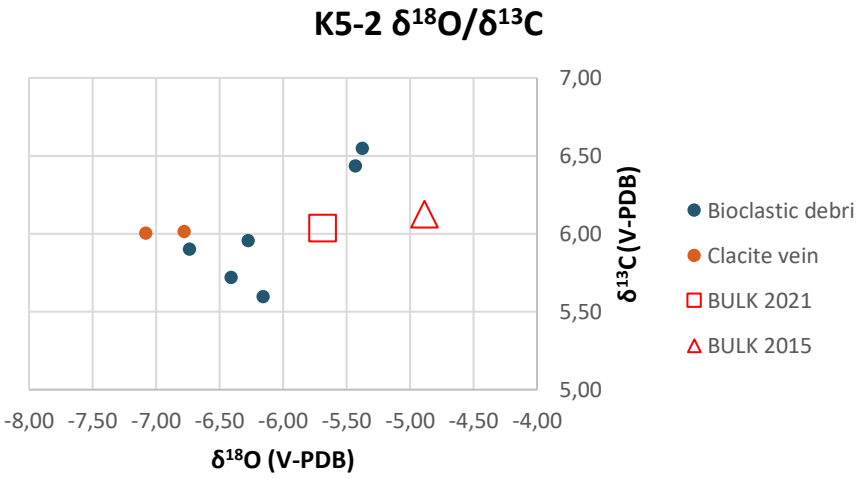

Figure 12. Cross-plot of $\delta^{18}O$ $\delta^{13}C$ values for K5-2. Results on micro-drilled samples are compared to previous bulk-rock results.

Sample K5-2 is a packstone composed of fine bioclastic debris and has a secondary calcite vein running through the sample. Sub-samples were micro-drilled from 6 spots that had a slight difference in coloration and from two areas along calcite vein (Figure 11). As shown on the graph (Figure 12), $\delta^{13}C$ ranges ~1‰ and $\delta^{18}O$ ~1.5‰. The bulk-rock $\delta^{13}C$ value is close to average value of micro-drilled sub-samples but bulk-rock $\delta^{18}O$ is slightly more positive compared to average value of micro-drilled sub-samples. Calcite veins exhibit compositions that are more depleted in ^{18}O.

Sample K1 is bioclastic grainstone (Figure 13). Sub-samples were micro-drilled from visually lighter parts (more debris) and darker parts (calcite crystals). Sub-sample 3 is taken from dolomitic part of the sample (Figure 8) yielding the most positive $\delta^{18}O$ value. Calcite dominated sub-samples exhibit ~1‰ variability for both $\delta^{13}C$ and $\delta^{18}O$ (Figure 14) and the bulk-rock values are close to averages on sub-samples. It can be seen that darker calcite crystal parts (1, 2 and 4) are slightly more depleted in ^{13}C compared to bioclastic debris.

Sample OP is lithologically most heterogeneous rudstone. It is composed of different fossil fragments and lithoclasts surrounded by matrix (cement, micrite, bioclastic debris). Micro-drilling was undertaken on different fossil fragments, ooids (1–9), recrystalized parts of putative stromatoporoids (16 and 17), unidentified fossil (10), lighter (14, 15) and darker lithoclasts (18, 19, 20) and matrix cement (11, 12, 13) (Figure 15). The $\delta^{13}C$ values range from about 2‰ to 7.5‰ and $\delta^{18}O$ from about 3 ‰ to 6.5‰ (Figure 16). Matrix $\delta^{13}C$ values are typically ~3‰ lower compared to clasts. Large stromatoporoid clast (16) exhibits the highest $\delta^{13}C$ value. Lithoclast values typically cluster within a narrow range, except one (19) that has 1‰ more positive $\delta^{18}O$ value. Whereas the $\delta^{13}C$ values of ooids are relatively stable but the $\delta^{18}O$ values are rather variable (~3.5‰). The isotope data on micro-drilled samples cluster around the bulk-rock value.

Placing the isotope results into the context of Mn variability among individual components as indicated by the µ-XRF map, a broad relationship between higher Mn and lower $\delta^{13}C$ values is observed (Figure 17). Note that the µ-XRF mapped thin sections and micro-drilled offcuts do not match exactly, hence the placement of micro-drilling spots on Mn map (Figure 17) is adjusted for best correspondence of components.

K1

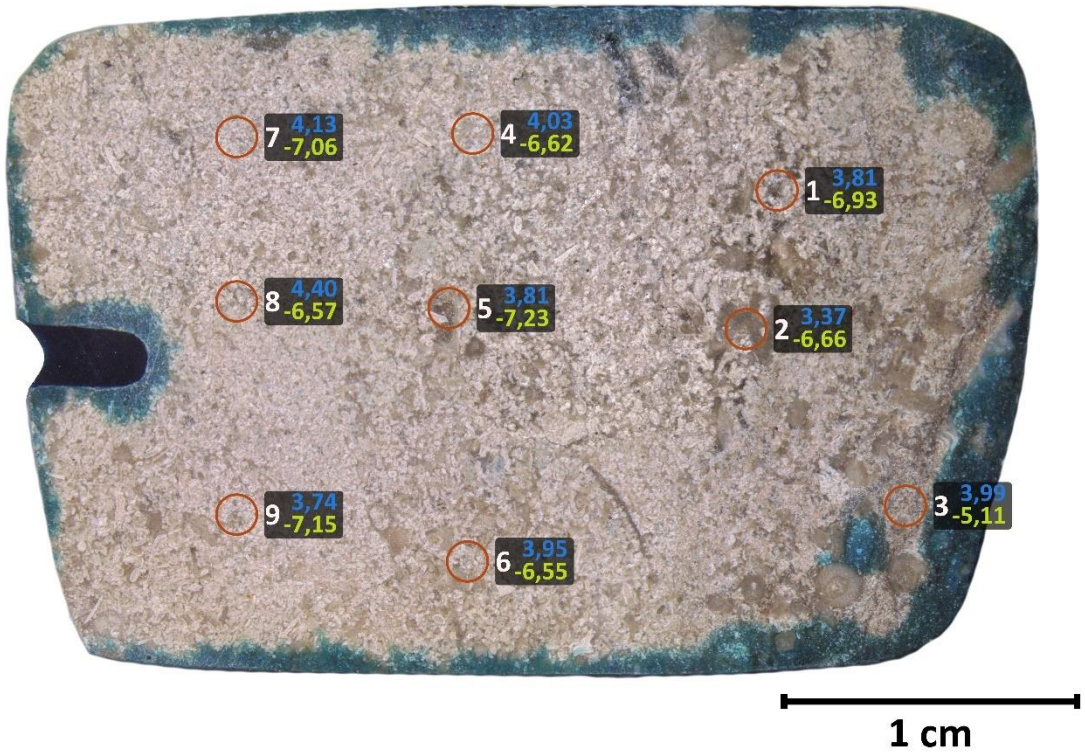

Figure 13. Optical image of K1 sample. Red circles correspond to micro-drilling spots and dark boxes list corresponding sample numbers (white), $\delta^{13}C$ values (blue), $\delta^{18}O$ values (green).

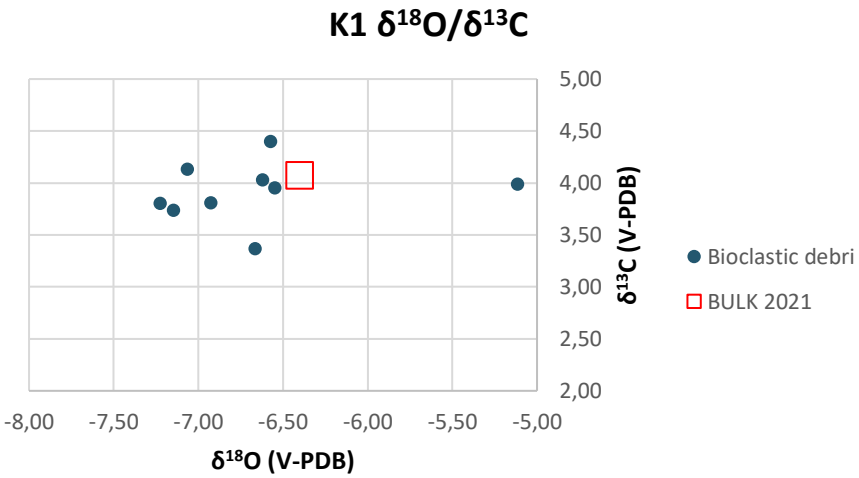

Figure 14. Cross-plot of $\delta^{18}O$ and $\delta^{13}C$ value for OP. Results on micro-drilled samples are compared to previous bulk-rock data.

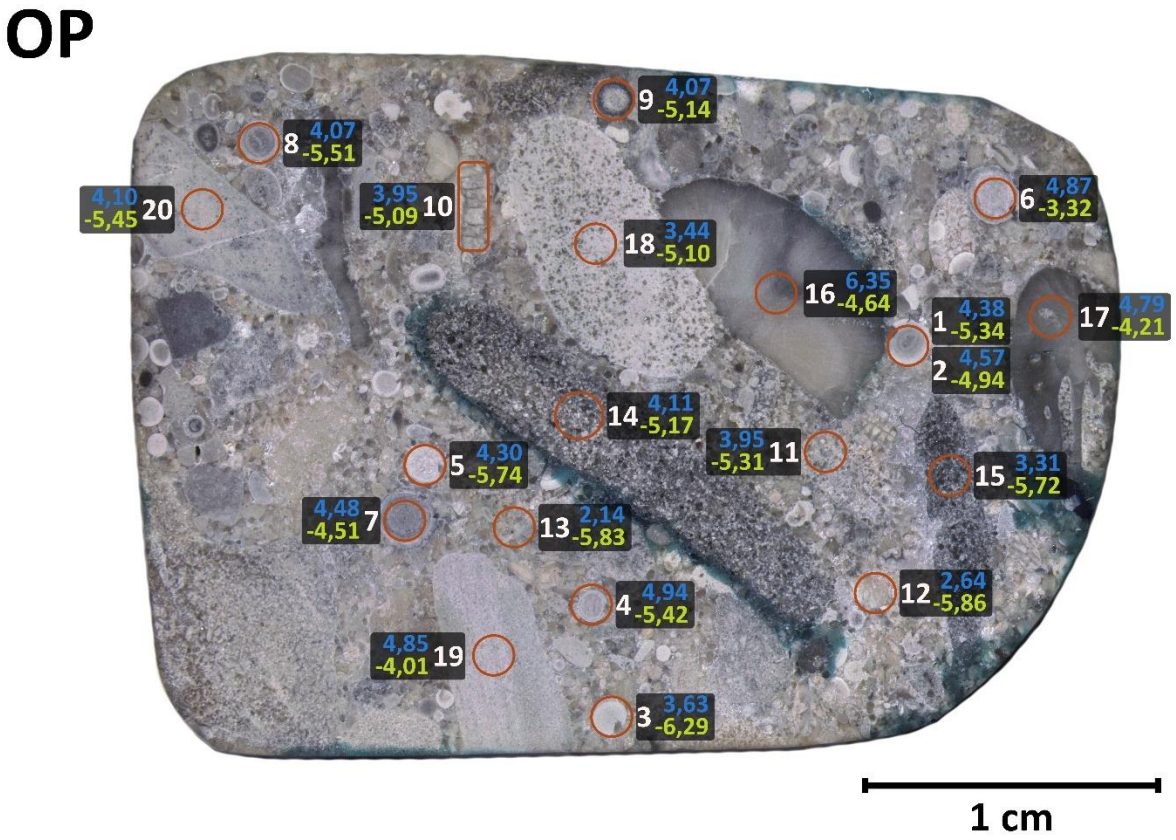

Figure 15. Optical image of OP sample. Red circles correspond to micro-drilling spots and dark boxes list corresponding sample numbers (white), $\delta^{13}C$ values (blue), $\delta^{18}O$ values (green).

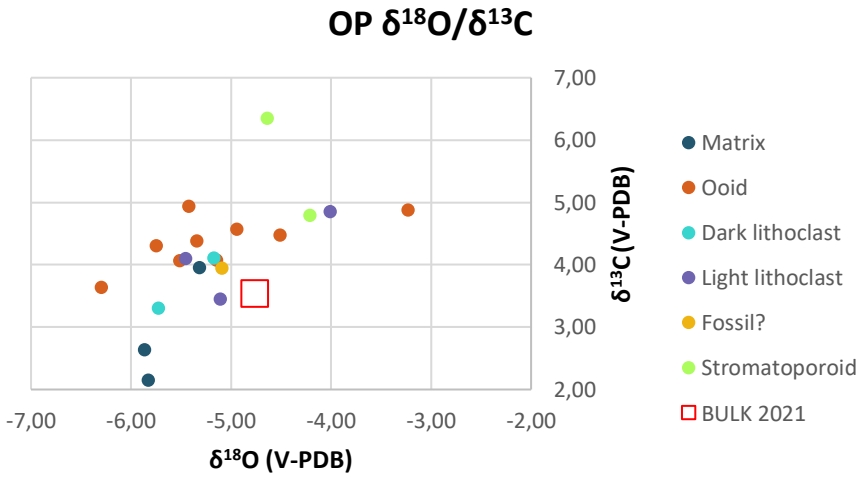

Figure 16. Cross-plot of $\delta^{18}O$ and $\delta^{13}C$ value for OP. Results on micro-drilled samples are compared to previous bulk-rock data.

This µ-XRF based observation was the basis for quantifying elemental abundances around micro-drilled spots with LA-ICP-MS. Three to four LA-ICP-MS measurements were taken around each micro-drilled spot and averages of these were used for cross plots of Mn and Sr against $\delta^{13}C$ and $\delta^{18}O$ (Figure 18; Table 4). Based on R^2 values shown in Figure 18, there is a very small correlation between Mn, Sr, $\delta^{13}C$ and $\delta^{18}O$. Little higher (R^2 = 0,19) covariance can be seen between Mn/Sr and $\delta^{13}C$. Based on amount of data and considering that there are many factors that can affect the true values used in these cross-plots, R^2 = 0,19 is still a basis for future studies with such data.

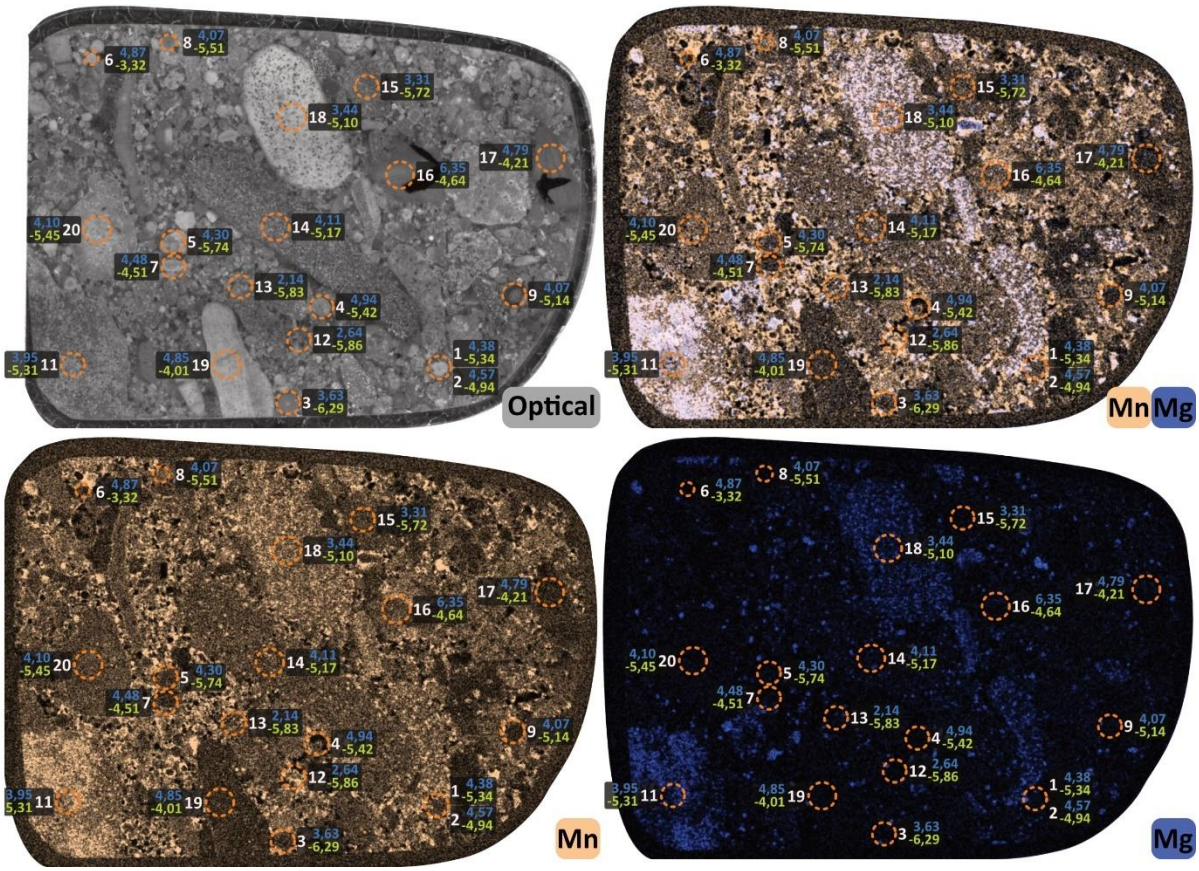

Figure 17. Optical image of studied sample (OP) thin sections and µ-XRF elemental maps for Mn and Mg. Dashed orange circles represent closest component on thin section in relation to offcut component. The brightest areas represent the highest measured cps.

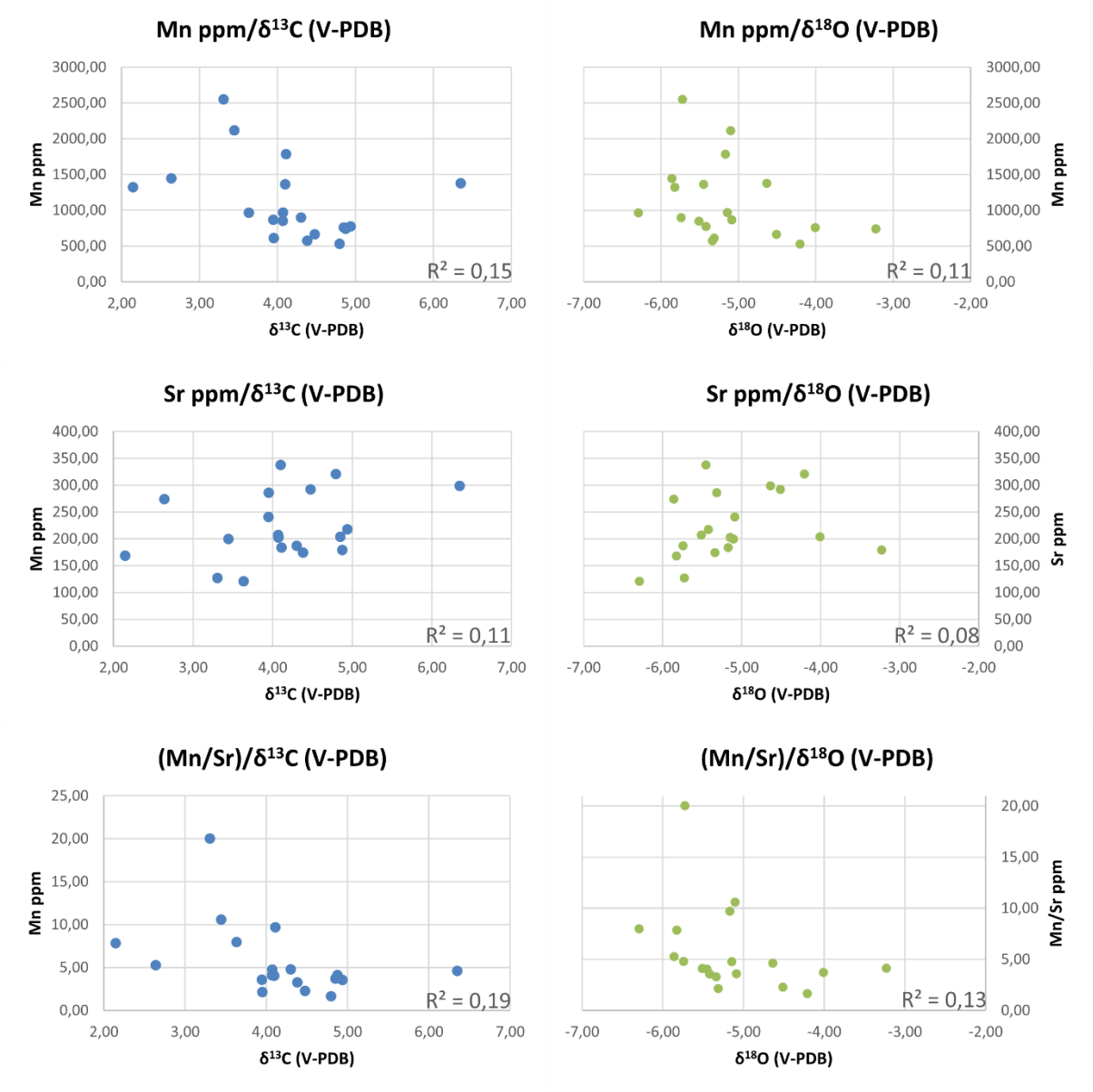

Figure 18. Cross-plots of Mn and Sr concentrations in ppm and Mn/Sr against $\delta^{18}O$ and $\delta^{13}C$ in studied OP sample.

Both VID-1 and VID-3 samples represent heterogeneous packstones which are composed of different fossils, mainly brachiopods, algae, ostracods and possibly other unidentified fossils surrounded by matrix (cement, micrite, bioclastic debris). Fossil type of each analysed component, was classified as accurately as possible. Many SIMS datapoints had to be rejected (Chapter 4), and only data classified as “Good” and “Warning” are used.

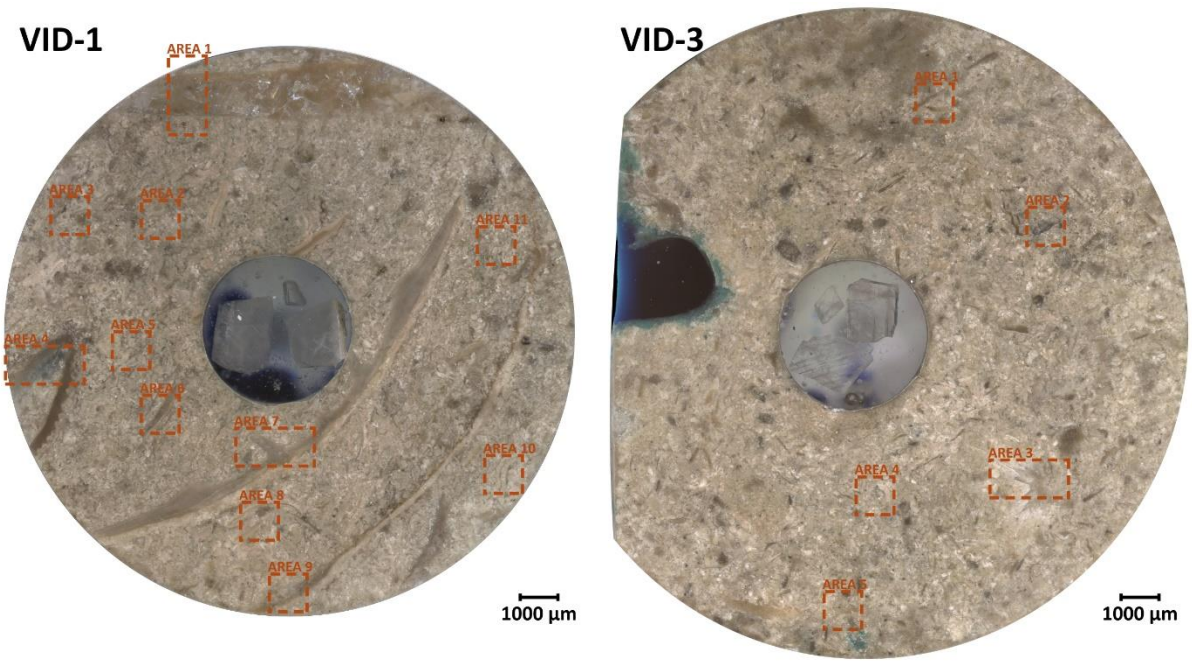

Figure 19. VID-1 and VID-3 sample with defined areas (red dashed boxes) where SIMS analyses were undertaken.

In spite of numerous rejected datapoints, the SIMS dataset on sample VID-1, is large enough to assess isotopic differences in various components. Locations of 11 defined areas in VID-1 are shown on Figure 19 and close-ups of these areas and positions of SIMS spots are shown on Figure 24. In addition to cross-plot of $\delta^{18}O$ and $\delta^{13}C$ that only contains data that meet the accepted criteria for both $\delta^{18}O$ and $\delta^{13}C$ (Figure 20), separate component specific plots for $\delta^{13}C$ and $\delta^{18}O$ using all accepted data were made to show variability within and between the component types (Figure 21). Altogether $\delta^{13}C$ varies ~5‰ and δ18O ~4.5‰. Bulk-rock $\delta^{13}C$ value is slightly more negative than SIMS average and bulk $\delta^{18}O$ value is close to SIMS average. In general, brachiopods (1, 4 and 6 in areas 1, 7, 6 respectively) and blocky calcite (surrounded by brachiopod 2 in area 4) have lower $\delta^{18}O$ values compared to matrix and data from algae and ostracods vary around average. For $\delta^{13}C$ values, algae seem to exhibit higher $\delta^{13}C$ values. Blocky calcite, brachiopod 2 that surrounds it (area 4) and brachiopod 4 have clearly lower $\delta^{13}C$ values but no clear grouping with other brachiopods can be seen. Algae is more enriched with ^{13}C compared to SIMS average.

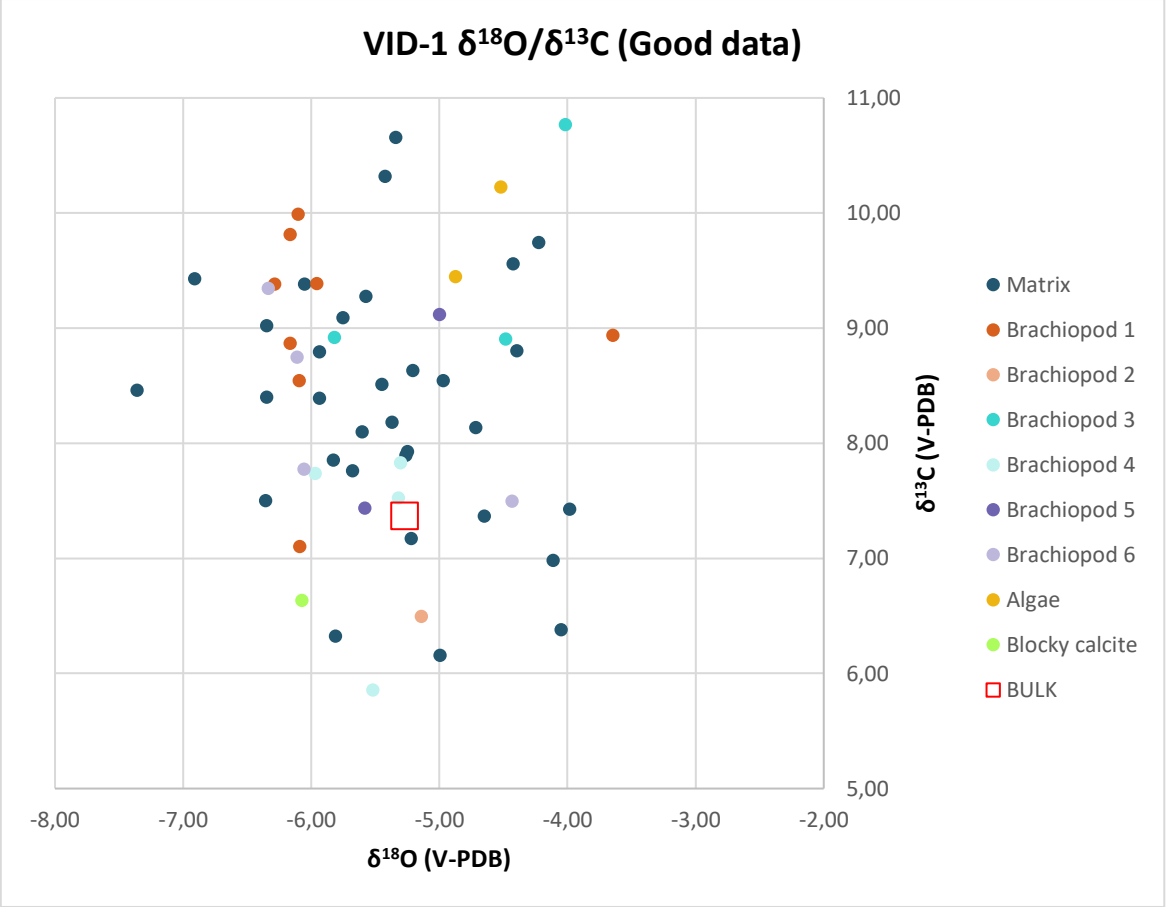

Figure 20. Cross-plot of $\delta^{18}O$ and $\delta^{13}C$ value for VID-1. Results on micro-drilled samples are compared to previous bulk-rock data (Martma, et al., 2005).

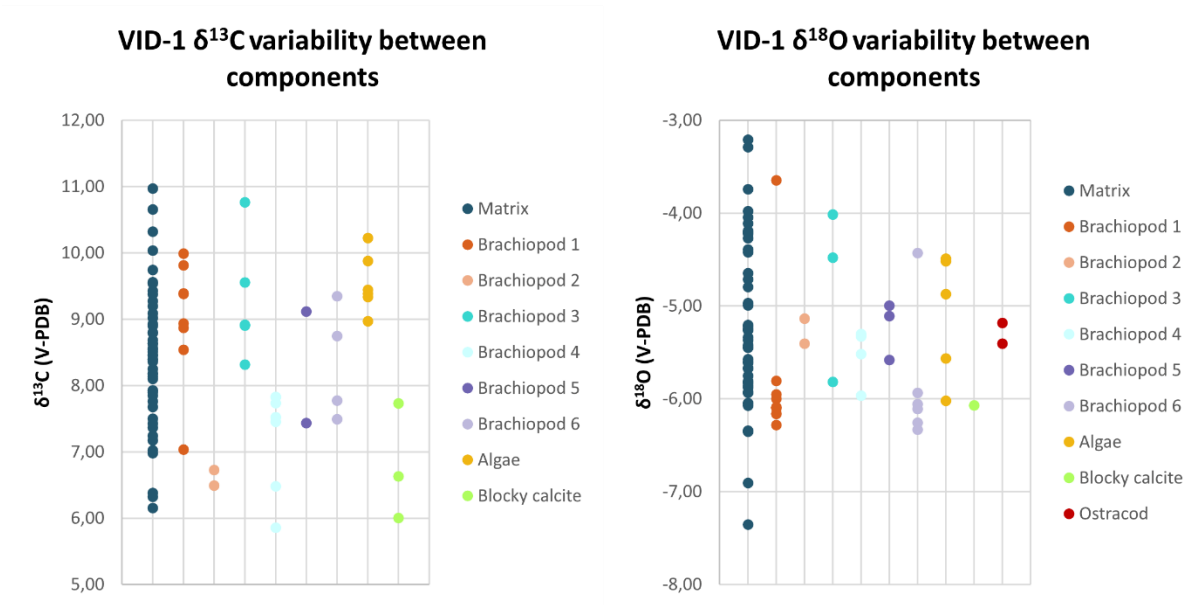

Figure 21. $\delta^{18}O$ and $\delta^{13}C$ variability between different components in studied sample VID-1.

7. Discussion

7.1 Sample-scale isotopic heterogeneity and its underlying causes

As highlighted in Chapters 2.2 and 2.3, various syn- and post-depositional processes can influence geochemical characteristics of carbonate sediments that may result in sample-scale isotopic heterogeneity. Data on higher Mg material have more positive $\delta^{18}O$ values (~1‰) compared to surrounding LMC as seen in samples K1 and in K5-1, i.e. more positive $\delta^{18}O$ values are seen in sub-samples taken from material that have higher Mg content (Figure 8). This agrees with laboratory studies by Tarutani, Clayton, & Mayeda, (1969) showing that in the same depositional conditions, HMC is enriched in ^{18}O compared to LMC. Data on sub-samples 7 and 8, taken from calcite vein in sample K5-2, exhibit more negative $\delta^{18}O$ values but similar $\delta^{13}C$ values compared to other sub-samples from K5-2. Calcite vein is clearly a secondary component that runs through the sample and both the vein and its host rock are composed of LMC. It is possible that the secondary fluid had a different $\delta^{18}O$ composition than the seawater from which the original material deposited. Given that the $\delta^{18}O$ value of a carbonate is inversely correlated to temperature (Swart, 2015), it is also possible that the vein fluids were warmer compared to temperature in which primary (host rock) material deposited.

Abundances of Mn and Sr are commonly used to evaluate diagenetic overprints as concentration of Mn increases and Sr decreases under diagenetic re-equilibration between different carbonate components and meteoric water (Brand & Veizer, 1980). Kaufman & Knoll, (1995) suggest that carbonates, both limestones and dolostones with Mn/Sr <10 commonly retain the near original carbon isotopic composition. The Mn/Sr ratios are below 10 in almost all components of sample OP, suggesting low diagenetic overprint and that the original isotopic composition of components can be preserved. However, lowest isotope ratios which partially correspond ($\delta^{13}C$ R^2 = 0,19; $\delta^{18}O$ R^2 = 0,13) to the components carrying highest Mn/Sr may be explained by variable diagenetic influence and post-depositional origin of components carrying the lowest $\delta^{13}C$ and $\delta^{18}O$ values. The difference in isotopic composition between components representing fossil fragments in OP sample may be caused by “vital effect” (Erez, 1978) and/or the nature and preservation of the material as thicker and denser material is more resistant to diagenesis (Grossman, *et al.,* 2008). However, the matrix that fills the pore space between bioclastic components, may include later forming

diagenetic material and/or matrix itself has undergone recrystallization that isotopically re-equilibrated pre-existing material (Cramer & Jarvis, 2020; Swart, 2015). More homogeneous samples (K5-1, K5-2 and K1) show less variability in $\delta^{13}C$ values (∼1‰) and slightly higher $\delta^{18}O$ values (∼2‰). Micro-drilled sub-samples of lithologically homogeneous (including fine-grained bioclatic debri which components can not be separated) materials are in essence bulk-rock measurements and slightly bigger variation in $\delta^{18}O$ are expected as $\delta^{18}O$ is highly variable in bulk-rock and that is why in O isotope stratigraphy, fossils and microfossils are preferred for more reliable data (Grossman & Joachimski, 2020). In case of OP sample, it is shown in Figure 16, that ooids are not reliable for O isotope stratigraphy, because on the sample-scale, $\delta^{18}O$ values vary ∼3‰.

7.2 Correspondence between bulk-rock and high spatial resolution isotope data and implications for bulk-rock interpretations

The results of the thesis show that even within small samples (HICE samples ∼30x20 mm and MLCIE samples ∼15 mm in diameter), $\delta^{13}C$ and $\delta^{18}O$ values can have large variations (∼4‰), especially if the samples are lithologically heterogeneous (VID-1, VID-3 and OP). For all studied samples the, bulk-rock values are typically more negative in $\delta^{13}C$ and more positive in $\delta^{18}O$ compared to micro-drilled or in-situ analysed sub-sample averages. When considering that carbonate diagenesis can result in post-depositional negative shifts of bulk-rock $\delta^{13}C$ values (Cramer & Jarvis, 2020) then magnitudes of $\delta^{13}C$ excursions can be much higher in sections where carbonate sediments are lithologically heterogeneous. This is clearly shown by sample OP, where $\delta^{13}C$ and $\delta^{18}O$ values of matrix and bulk-rock are 2–3‰ lower compared bioclasts. It can be argued that $\delta^{13}C$ and $\delta^{18}O$ relationships in OP forming L-shaped trend and progressively lower values, tracks post-depositional alteration (Figure 22). The data can be divided into three groups including components that (i) carry best-preserved, possibly primary values ($\delta^{13}C$ ∼5‰ and $\delta^{18}O$ ∼-3.5‰), (ii) have experienced resetting of oxygen and shift towards lower $\delta^{18}O$ values with limited effect on $\delta^{13}C$ values ($\delta^{13}C$ ∼4 to 5‰ and $\delta^{18}O$ ∼-5.5 to -4‰) and are strongly affected by diagenetic (re)crystallization ($\delta^{13}C$ ∼2 to 4‰ and $\delta^{18}O$ ∼-6.5 to -5.5‰). Mn/Sr that can be used for assessing the degree of diagenetic overprint which partially correlates ($\delta^{13}C$ R^2 = 0,19; $\delta^{18}O$ R^2 = 0,13) with the trend towards lower values.

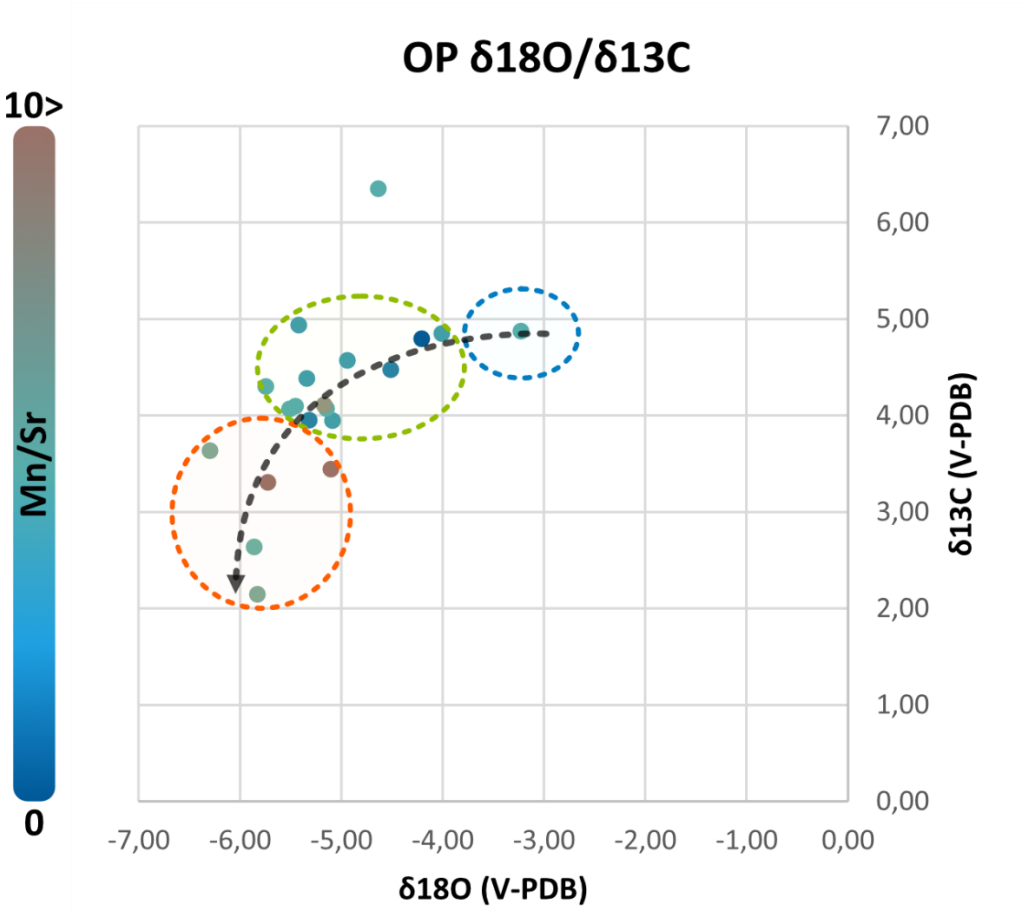

Figure 22. Cross-plot of $\delta^{18}O$ and $\delta^{13}C$ values for OP. Data points on chart are coloured based on Mn/Sr. Black dashed arrow shows a L-shaped trend interpreted to track isotopic changes of post-depositional alteration. Three outlined ellipses representing: best-preserved components carrying primary signal (blue dashed ellipse), components experiencing oxygen isotope resetting (green dashed ellipse) and components strongly influenced by diagenetic resetting and (re)crystallization (red dashed ellipse).

Similar variation in $\delta^{18}O$ (~3–4‰) has been shown before by Goldberg, *et al.,* (2021), combined $\delta^{18}O$ data shows that bulk-rock varies ~3‰ consistently between Cambrian and beginning of Silurian but $\delta^{18}O$ data derived from fossils show that from around middle of the Ordovician, $\delta^{18}O$ variability increases towards Silurian and ~3‰ $\delta^{18}O$ variance is also seen in sample OP that represents end of the Ordovician. Samples VID-1 and VID-3 represent heterogeneous material packstones, but matrix values are not lower than other distinct components. Some of the components show a grouping of values but the ranges within which these components values vary, are not always same between components of the same type

classification i.e., brachiopods. This can be the result of inaccurate classifications of components and/or inability to separate specific components as dimensions are too small. Another possibility for components not having distinct values, is variable preservation of the fossils discussed above. What is clearly seen in case of VID-1, is that all the distinct components are within the range, clustering around matrix $\delta^{13}C$ and $\delta^{18}O$ values. Comparison of the new component specific data with previous bulk results, demonstrates that in studied Vidukle 61 drill core, individual components are as much as 4‰ heavier ($\delta^{13}C$ as high as 12‰) than the bulk-rock values (8‰; Figure 23).

The results show that heterogeneous carbonate sediment can exhibit significant $\delta^{13}C$ differences between distinct components (OP) and the range of $\delta^{13}C$ values of components can overlap with the range seen in matrix (VID-1 and VID-3). The high spatial resolution data reveal the presence of several components carrying higher $\delta^{13}C$ values than the bulk rock and allow more accurately determine the magnitudes of positive $\delta^{13}C$ excursions. Figure 23 illustrates how much the magnitude of excursions can vary in different components compared to bulk-rock. Still, bulk-rock analysis on the micritic samples without distinct separable components (K1, K5-1 and K5-2), provide accurate $\delta^{13}C$ values within ~1‰. In case of grainstones and packstones, containing distinct components that are too small to be micro-drilled (VID-1 and VID-3), in-situ analysis (such as SIMS) allow assessment of component specific sample-scale isotopic heterogeneity. Micro-drilling from most fine-grained areas is suggested because in samples VID-1 and VID-3, matrix $\delta^{13}C$ values cover the range of different fossil component values and in-situ analysis can be complicated on fine-grained material. In case of samples which have components big enough (OP) for micro-drilling, sub-samples should be taken from enclosed fossils that are likely to preserve best preserve the original isotopic characteristics. These type of assessments can help to keep sample count lower while still providing the data on best preserved components for robust reconstruction of $\delta^{13}C$ curves.

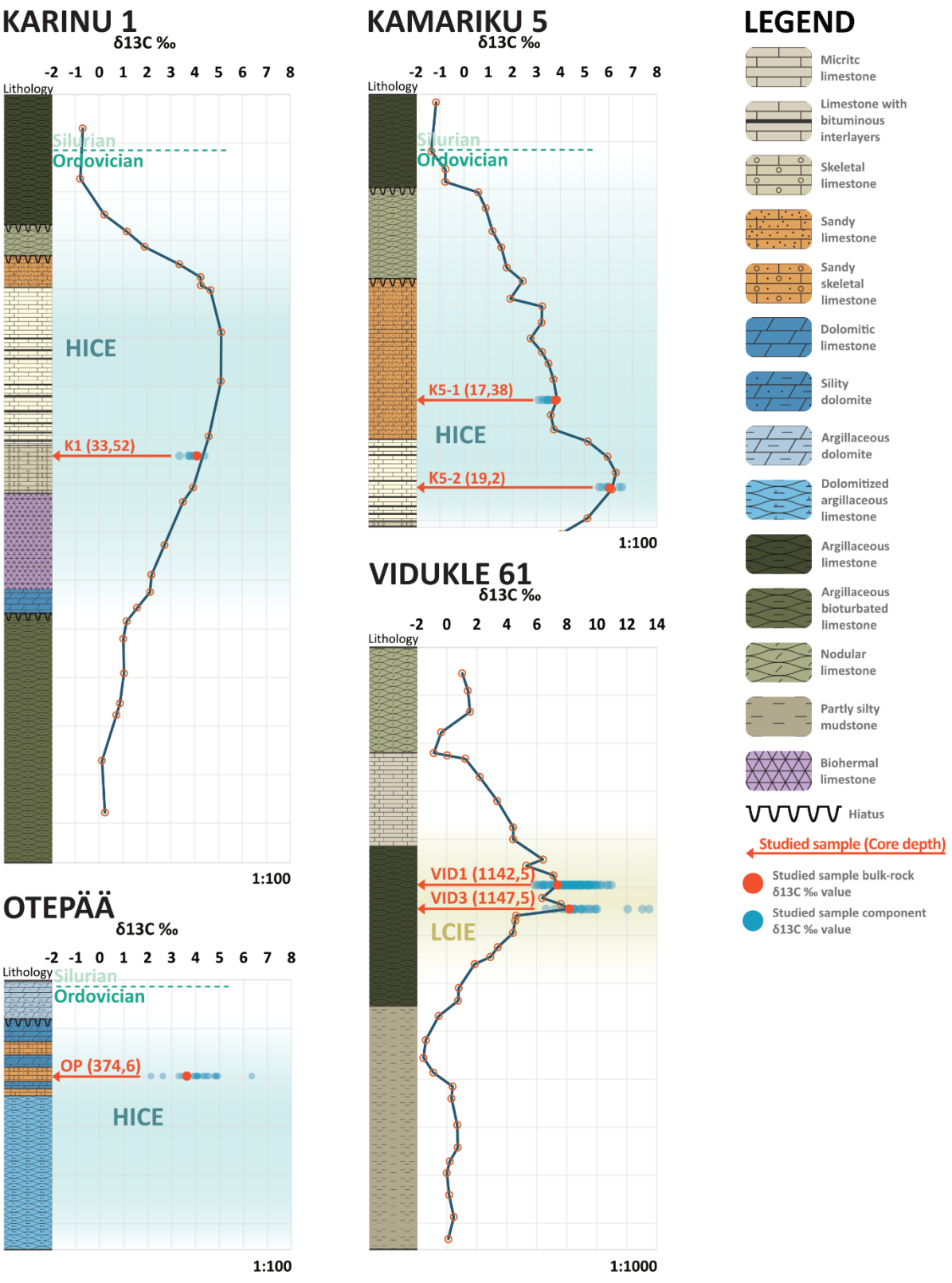

Figure 23. Comparison of component specific $\delta^{13}C$ values obtained in this thesis with previous bulk-rock results. Limited sample-scale heterogeneity and good correspondence with bulk-rock values is seen in micritic samples whereas wacke- and grainstone samples exhibit up to 5‰ range of $\delta^{13}C$ values with several components up to 3‰ heavier than the bulk-rock values.

8. Summary

This thesis focused on determining sample-scale isotopic heterogeneity of Palaeozoic carbonate rocks in intervals housing prominent global $\delta^{13}C$ excursions, the Hirnantian Isotopic Carbon Excursion (HICE) and the Mid-Ludfordian Carbon Isotope Excursions (MLCIE). The results show that deviation of different rock component composition from average and bulk-rock value increases with the increase of lithological heterogeneity of analysed material. The variability of $\delta^{13}C$ and $\delta^{18}O$ can be significant even in small lithologically heterogeneous samples (~15–30 mm). Limited sample-scale heterogeneity and good correspondence with bulk-rock $\delta^{13}C$ values is seen in micritic samples whereas wacke- and grainstone samples exhibit up to 5‰ range of $\delta^{13}C$ values with several components up to 3‰ heavier than the bulk-rock values.

There are few types of assessments that can help to keep sample count lower while still providing the data on best preserved components for robust reconstruction of $\delta^{13}C$ curves. (i) Bulk-rock analysis on the micritic samples without distinct separable components provide accurate values within ~1‰. (ii) Grainstones and packstones with small grain size, such as studied samples VID-1 and VID-2, which are composed of components that are too small to be micro-drilled, in-situ analysis (such as SIMS) allow assessment of component specific sample-scale isotopic heterogeneity but micro-drilling from most fine-grained areas of such material is suggested because matrix $\delta^{13}C$ values cover the range of different component values and in-situ analysis can be complicated on fine-grained sedimentary material. (iii) Samples which have components big enough (OP) for micro-drilling, sub-samples should be taken from enclosed fossils that best preserve the original isotopic characteristics.

Both in Ordovician and more so in Silurian samples, no clear grouping of data on $\delta^{18}O/\delta^{13}C$ cross-plots can be seen. This can be caused by differences in sample preservation and/or inability to separate or classify specific components as dimensions are too small. To better define how different components preserve their isotopic signal, further studies on larger range of lithologically heterogenous materials should be done.

In sample OP relatively low Mn/Sr ratios (<10) suggest that some components are slightly affected by meteoric waters. L-trend can be seen in $\delta^{18}O$ vs $\delta^{13}C$ cross-plot and it can be argued that it tracks post-depositional alteration. The data can be divided into three groups

including components that (i) carry best-preserved, possibly primary values, (ii) have experienced resetting of oxygen and shift towards lower $\delta^{18}O$ values with limited effect on $\delta^{13}C$ values and (iii) are strongly affected by diagenetic (re)crystallization. Mn/Sr that is used for assessing the degree of diagenetic overprint, partially correlates ($\delta^{13}C$ R^2 = 0,19; $\delta^{18}O$ R^2 = 0,13) with the trend towards lower isotope ratio values. Given the tendency of diagenetic alteration to cause a shift towards lower values, the range (~3‰) of $\delta^{18}O$ values can be explained by incomplete diagenetic overprint. Such ranges of carbonate $\delta^{18}O$ values have been reported before in Ordovician and Silurian successions.

Kokkuvõte

See lõputöö keskendus Paleosoikumi proovi-skaalas karbonaatkivimite isotoopkoostise heterogeensuse määramisele, kivimite intervallidest, mis esindavad globaalseid $\delta^{13}C$ ekskursioone, Hirnanti Süsiniku Isotoobi Ekskursioon (HICE) ja Kesk-Ludfordi Süsiniku Isotoobi Ekskursioon. Tulemused näitavad, et erinevate kivimkomponentide koostise hajuvus keskmisest ning täiskivimi väärtusest suureneb koos analüüsitud materjalide litoloogilise heterogeensuse suurenemisega. $\delta^{13}C$ ja $\delta^{18}O$ varieeruvus võib olla märkimisväärne isegi väikestes litoloogiliselt heterogeensetes proovides (∼15–30 mm). Piiratud heterogeensust proovi-skaalas ja head vastavust täiskivimi $\delta^{13}C$ väärtustega on näha mikriitsetes proovides, samas kui mudalis-teraliste ja teraliste lubjakivi proovide $\delta^{13}C$ väärtuste vahemik on kuni 5‰ ning mitmete komponentide väärtused on kuni 3‰ raskemad kui täiskivimi väärtused.

Litoloogiliselt erinevatele proovidele tehtud uuringu tulemusena on võimalik anda enne proovide analüüsimist hinnang, vähendades proovide arvu ning samal ajal säilitades andmete usalduväärsus, et rekonstrueerida $\delta^{13}C$ kõveraid, mis võiksid täpsemini peegeldada settimisaegseid tingimusi. (i) Mikriitsetele proovidele täiskivimi analüüside tegemisel, millel pole selgesti eristatavaid komponente, saab väärtuseid ∼1‰ täpsusega. (ii) Väikese tera suurusega mudalis-teraliste ja teraliste lubjakivi, nagu uuritud proovid VID-1 ja VID-2, mis koosnevad mikropuurimiseks liiga väikestest komponentidest, on võimalik mõõta in-situ anlaüüsmeetoditega (nt SIMS-ga), et hinnata proovi-skaalas komponentide põhiselt isotoopilist heterogeensust, kuid on soovitatav teha mikropuurimisi sellise materjali mõnest kõige peeneteralisematest piirkondadest, kuna komponentide $\delta^{13}C$ väärtused jäävad maatriksi $\delta^{13}C$ väärtuste vahemikku ja peeneteralise settematerjali puhul võib in-situ analüüside teostamine olla keeruline. (iii) Proovide korral, mille komponendid (OP) on mikropuurimiseks piisavalt suured, tuleks alamproovid võtta ümbritsetud fossiilidest, mis säilitavad kõige paremini algseid isotoopsignaale.

Nii Ordoviitsiumi ning veelgi enam Siluri ajastu proovides ei ole näha $\delta^{18}O$ vs $\delta^{13}C$ ristdiagrammidel andmete selget rühmitust. Selle põhjuseks võivad olla proovide säilimise erinevused ja/või võimetus eraldada või klassifitseerida konkreetseid komponente, kuna mõõtmed on liiga väikesed. Et paremini määratleda, kuidas erinevad komponendid säilitavad oma isotoopsignaali, tuleks teha täiendavaid uuringuid suuremal hulgal litoloogiliselt heterogeensetel materjalidel.

Proovis OP, Mn ja Sr suhted (<10) näitavad, et mõned kivimi komponendid on ainult natuke mõjutatud meteoorsest veest. $\delta^{18}O$ vs $\delta^{13}C$ ristdiagrammil on näha L-trendi ja võib argumenteerida, et see järgib settimise järgseid muutuseid. Andmed võib jagada kolme rühma, sealhulgas komponendid, mis (i) kannavad kõige paremini säilinud, võimalik, et esmaseid isotoopväärtuseid, (ii) on läbinud hapniku uuenemist ja nihkunud madalamate $\delta^{18}O$ väärtuste poole, millel on piiratud mõju $\delta^{13}C$ väärtustele ja (iii) on tugevalt mõjutatud diageneetiliselt (ümber)kristalliseerumise teel. Mn/Sr, mida kasutatakse diageneetilise mõju ulatuse näitamiseks, läheb õrnalt kokku ($\delta^{13}C$ R^2 = 0,19; $\delta^{18}O$ R^2 = 0,13) trendiga madalamate isotoopsuhete väärtuste suunas. Arvestades diageneetiliste muutuste kalduvust madalamate väärtuste poole, saab $\delta^{18}O$ väärtuste ulatust (∼3‰) seletada pooliku diagneesist põhjustatud isotoopväärtuste uuenemisega. Selliseid variatsioone on täheldatud ka varasemalt Ordoviitsiumis ja Siluris. Lisaks võib kõrgema magneesiumi sisaldusega materjalides näha rikastumist ^{18}O-ga (∼1 ‰), mida toetavad varasemad uuringud.

Acknowledgments

I want to thank my supervisors Leho Ainsaar and Aivo Lepland for giving me an opportunity to carry out the study on this topic. I am grateful to Holar Sepp who helped with creating a workflow for sample preparation for IRMS and for showing me how the IRMS machine works. I am also grateful to Päärn Paiste for teaching me the principles of LA-ICP-MS and for giving me the opportunity to be part of the analysis done with it. Furthermore, I really want to thank Alicja Wudarska for being a link between us and German Research Centre for Geosciences lab in Potsdam where isotopic analysis was carried out by SIMS and for explaining on how documentation should be done for analysis and for meticulous screening and quality control of the measurements.

References

Ainsaar, L., Meidla, T., & Hints, O. (2019). Carbon isotopic compostion of Ordovician carbonates in Baltoscandia : shallow marine facies shifting the δ13Ccarb values in different ways. In O. T. Obut, N. V. Sennikov, & T. P. Kipriyanova, *13th International Symposium on the Ordovician System : Novosibirsk, Russia (July 19-22, 2019) : contributions* (pp. 7-8). Novosibirsk: Publishing House of SB RAS. doi:10.15372/INTERNATIONAL2019OOT

Ainsaar, L., Truumees, J., & Meidla, T. (2015). The Position of the Ordovician–Silurian Boundary in Estonia Tested by High-Resolution δ13C Chemostratigraphic Correlation. In M. Ramkumar, *Chemostratigraphy: Concepts, Techniques, and Applications* (pp. 395-412). Elsevier. doi:10.1016/b978-0-12-419968-2.00015-7

Allan, J. R., & Matthews, R. K. (1982). Isotope signatures associated with early meteoric diagenesis. *Sedimentology, XXIX*(6), 797-817. doi:10.1111/j.1365-3091.1982.tb00085.x

Allison, C. E., Francey, R. J., & Meijer, H. A. (1995). Reference and intercomparison materials for stable isotopes of light elements. *IAEA-TECDOC-825* (pp. 155-162). Vienna: IAEA. Retrieved 2022, from https://www.iaea.org/publications/5471/reference-and-intercomparison-materials-for-stable-isotopes-of-light-elements

Bachan, A., Lau, K. V., Saltzman, M. R., Thomas, E., Kump, L. R., & Payne, J. L. (2017, June). A model for the decrease in amplitude of carbon isotope excursions across the phanerozoic. *American Journal of Science, CCCXVII*, 641-676. doi:10.2475/06.2017.01

Baertschi, P. (1976). Absolute18O content of standard mean ocean water. *Earth and Planetary Science Letters, XXXI*(3), 341-344. doi:10.1016/0012-821X(76)90115-1

Brand, U. (1982). The oxygen and carbon isotope composition of carboniferous fossil components: sea-water effects. *Sedimentology*, 139-147. doi:10.1111/j.1365-3091.1982.

Brand, U., & Veizer, J. (1980). Chemical diagenesis of a multicomponent carbonate system - 1. Trace elements. *Journal of Sedimentary Research, L*(4), 1219-1236. doi:10.1306/212F7BB7-2B24-11D7-8648000102C1865D

Brand, W. A., Coplen, T. B., Vogl, J., Rosner, M., & Prohaska, T. (2014). Assessment of International Reference Materials for Stable Isotope Ratio Analysis 2013 (IUPAC Technical Report). *Pure and Applied Chemistry, LXXXVI*(3), 425. doi:10.1515/pac-2013-1023

Cocks, L. R., & Torsvik, T. H. (2005). Baltica from the late Precambrian to mid-Palaeozoic times: The gain and loss of a terrane's identity. *Earth-Science Reviews, LXXII*(1-2), 39-66. doi:10.1016/j.earscirev.2005.04.001

Craig, H. (1957). Isotopic standards for carbon and oxygen and correction factors for mass-spectrometric analysis of carbon dioxide. *Geochimica et Cosmochimica Acta, XII*(1-2), 133-149. doi:10.1016/0016-7037(57)90024-8

Cramer, B. D., & Jarvis, I. (2020). Carbon Isotope Stratigraphy. In F. M. Gradstein, J. G. Ogg, M. D. Schmitz, & G. M. Ogg, *Geologic Time Scale 2020* (pp. 309-343). Elsevier. doi:10.1016/B978-0-12-824360-2.00011-5

Cramer, B. D., Vandenbroucke, T. R., & Ludvigson, G. A. (2015). High-Resolution Event Stratigraphy (HiRES) and the quantification of stratigraphic uncertainty: Silurian examples of the quest for precision in stratigraphy. *Earth-Science Reviews, CXLI*, 136-153. doi:10.1016/j.earscirev.2014.11.011

Erez, J. (1978). Vital effect on stable-isotope composition seen in foraminifera and coral skeletons. *Nature, CCLXXIII*, 199-202. doi:10.1038/273199a0

Frýda, J., Lehnert, O., Joachimski, M. M., Männik, P., Kubaijko, M., Mergl, M., . . . Frýdova, B. (2021). The Mid-Ludfordian (late Silurian) Glaciation: A link with global changes in ocean chemistry and ecosystem overturns. *Earth-Science Reviews*(CCXX), 1-32. doi:10.1016/j.earscirev.2021.103652.

Goldberg, S. L., Present, T. M., Finnegan, S., & Bergamann, K. D. (2021). A high-resolution record of early Paleozoic climate. *EARTH, ATMOSPHERIC, AND PLANETARY SCIENCES, CXVIII*(6), 1-8. doi:10.1073/pnas.2013083118

Goldman, D., Sadler, P. M., Leslie, S. A., Melchin, M. J., Agterberg, F. P., & Gradstein, F. M. (2020). The Ordovician Period. In F. M. Gradstein, J. G. Ogg, M. D. Schmitz, & G. M. Ogg, *Geologic Time Scale 2020* (Vol. II, pp. 631-694). Elsevier. doi:10.1016/B978-0-12-824360-2.00020-6

Grossman, E. L., & Joachimski, M. M. (2020). Oxygen Isotope Stratigraphy. In F. M. Gradstein, J. G. Ogg, M. D. Schmitz, & G. M. Ogg, *Geological Time Scale 2020* (pp. 279-307). Elsevier. doi:10.1016/B978-0-12-824360-2.00010-3

Grossman, E. L., Yancey, T. E., Jones, T. E., Bruckschen, P., Chuvashov, B., Mazzullo, S. J., & Mii, H. (2008). Glaciation, aridification, and carbon sequestration in the Permo-Carboniferous: The isotopic record from low latitudes. *Palaeogeography, Palaeoclimatology, Palaeoecology, CCLXVIII*, 222-233. doi:10.1016/j.palaeo.2008.03.053

Gruber, N., Keeling, C. D., Bacastow, R. B., Guenther, P. R., Lueker, T. J., Wahlen, M., . . . Stocker, T. F. (1999). Spatiotemporal patterns of carbon-13 in the global surface oceans and the oceanic Suess effect. *Global Biogeochemical Cycles, XIII*(2), 307-335. doi:10.1029/1999GB900019

Gul, B., Ainsaar, L., & Meidla, T. (2021). Latest Ordovician–early Silurian palaeoenvironmental changes and palaeotemperature trends indicated by stable carbon and oxygen isotopes from northern Estonia. *Estonian Journal of Earth Sciences, LXX*(4), 196-209. doi:10.3176/earth.2021.14

Hints, L., & Meidla, T. (1997). Porkuni Stage. In A. Raukas, & A. Teedumäe, *Geology and Mineral Resources of Estonia* (pp. 85-88). Tallinn: Estonian Academy Publishers. Retrieved from https://geoloogia.info/geology/

Hints, L., Hints, O., Kaljo, D., Kiipli, T., Männik, P., Nõlvak, J., & Pärnaste, H. (2010). Hirnantian (latest Ordovician) bio- and chemostratigraphy of the Stirnas-18 core, western Latvia. *Estonian Journal of Earth Sciences, LIX*(1), 1-24. doi:10.3176/earth.2010.1.01

Jaanusson, V. (1973). Aspects of carbonate sedimentation in the Ordovician of Baltoscandia. *Lethaia, VI*(1), 11-34. doi:10.1111/j.1502-3931.1973.tb00871.x

Kaufman, A. J., & Knoll, A. H. (1995). Neoproterozoic variations in the C-isotopic composition of seawater: stratigraphic and biogeochemical implications. *Precambrian Research, LXXIII*(1-4), 27-49. doi:10.1016/0301-9268(94)00070-8

Kozdon, R., Ushikubo, T., Kita, N. T., Spicuzza, M., & Valley, J. W. (2009). Intratest oxygen isotope variability in the planktonic foraminifer N. pachyderma: Real vs. apparent vital effects by ion microprobe. *Chemical Geology*, 327-337. doi:10.1016/j.chemgeo.2008.10.032

Lazauskiene, J., Stephenson, R., Šliaupa, S., & van Wees, J.-D. (2002). 3-D flexural modelling of the Silurian Baltic Basin. *Tectonophysics, CCCXLVI*, 115-135. doi:10.1016/S0040-1951(01)00231-1

Martma, T. (2022). *Sample No. 185844.* Department of Geology, TalTech. Tallinn: e-Maapõu. Retrieved from https://geoloogia.info/en/sample/185844/185844

Martma, T. (2022). *Sample No. 185848.* Department of Geology, TalTech. Tallinn: e-Maapõu. Retrieved from https://geoloogia.info/en/sample/185848/185848

Martma, T., Brazausaks, A., Kaljo, D., Kaminskas, D., & Musteikis, P. (2005). The Wenlock-Ludlow carbon isotope trend in the Vidukle core, Lithuania, and its relations with oceanic events. *Geological Quarterly, XLIX*(2), 223-234.

Melchin, M. J., Mitchell, C. E., Holmden, C., & Storch, P. (2013). Environmental changes in the Late Ordovician-early Silurian: Review and new insights from black shales and nitrogen isotopes. *Geological Society of America Bulletin, CXXV*(11-12), 1635-1670. doi:10.1130/B30812.1

Melchin, M. J., Sadler, P. M., & Cramer, B. D. (2020). The Silurian Period. In F. M. Gradstein, J. G. Ogg, M. D. Schmitz, & G. M. Ogg, *Geologic Time Scale 2020* (Vol. II, pp. 695-732). Elsevier. doi:10.1016/B978-0-12-824360-2.00021-8

Mook, W. G., Bommerson, J. C., & Staverman, W. H. (1974). Carbon isotope fractionation between dissolved bicarbonate and gaseous carbon dioxide. *Earth and Planetary Science Letters, XXII*(22), 169-176. doi:10.1016/0012-821x(74)90078-8

Nõlvak, J. (1997). Ordovician. Introduction. In A. Raukas, & A. Teedumäe, *Geology and mineral resources of Estonia* (pp. 54-55). Tallinn: Estonian Academy Publishers. Retrieved from https://geoloogia.info/geology/index.html

Oehlert, A. M., Lamb-Wozniak, K. A., Delvin, Q. B., Mackenzie, G. J., Reijmer, J. J., & Swart, P. K. (2012). The stable carbon isotopic composition of organic material in platform derived sediments: implications for reconstructing the global carbon cycle. *Sedimentology, LIX*(1), 319-335. doi:10.1111/j.1365-3091.2011.01273.x

Oraspõld, A. (1975). Литология поркуниского горизонта в Эстонии [Lithology of Porkuni Stage in Estonia]. *Tartu Riikliku Ülikooli Toimetised, CCCLIX*, 33-75.

Popp, B. N., Anderson, T. F., & Sandberg, P. A. (1986). Brachiopods as indicators of original isotopic compositions in some Paleozoic limestones. *Geological Society of America Bulletin, XCVII*, 1262-1269. doi:10.1130/0016-7606(1986)97,1262:BAIOOI.2.0.CO;2.

Rocha, D., & Passow, U. (2014). The Biological Pump. In H. D. Holland, & K. K. Turekian, *Treatise on Geochemistry* (2nd ed., Vol. IIX, pp. 93-122). Elsevier. doi:10.1016/B978-0-08-095975-7.00604-5

Romanek, C. S., Grossmann, E. L., & Morse, J. W. (1992). Carbon isotopic fractionation in synthetic aragonite and calcite: Effects of temperature and precipitation rate. *Geochimica et Cosmochimica Acta, LVI*(1), 419-430. doi:10.1016/0016-7037(92)90142-6

Saltzman, M. R., & Thomas, E. (2012). Carbon Isotope Stratigraphy. In F. M. Gradstein, J. G. Ogg, M. D. Schmitz, & G. M. Ogg, *The Geological Time Scale* (pp. 207-232). Elsevier. doi:10.1016/B978-0-444-59425-9.00011-1

Sarmiento, J. L., & Gruber, N. (2006). Ocean Biogeochemical Dynamics. *Geological Magazine*, p. 503 pp. doi:10.1017/S0016756807003755

Scotese, C. R. (2014). *Atlas of Silurian and Middle-Late Ordovician Paleogeographic Maps (Mollweide Projection), Maps 73 – 80, Volume 5, The Early Paleozoic, PALEOMAP Atlas for ArcGIS, PALEOMAP Project, Evanston, IL.* doi:10.13140/2.1.1087.2324

Spiridonov, A., Samsone, J., Brazauskas, A., Stankevic, R., Meidla, T., Ainsaar, L., & Radzevicius, S. (2020). Quantifying the community turnover of the uppermost Wenlock and Ludlow (Silurian) conodonts in the Baltic Basin. *Palaeogeography, Palaeoclimatology, Palaeoecology, DXLIX*. doi:10.1016/j.palaeo.2019.03.029.

Swart, P. K. (2015). The Geochemistry of Carbonate Diagenesis: The Past, Present and Future. *Sedimentology, LXII*(5), 1233-1304. doi:10.1111/sed.12205

Swart, P. K., & Oehlert, A. M. (2018). Revised interpretations of stable C and O patterns in carbonate rocks resulting from meteoric diagenesis. *Sedimentary Geology, CCCLXIV*, 14-23. doi:10.1016/j.sedgeo.2017.12.005

Tarutani, T., Clayton, R. N., & Mayeda, T. K. (1969). The effect of polymorphism and magnesium substitution on oxygen isotope fractionation between calcium carbonate and water. *Geochimica et Cosmochimica Acta, XXXIII*(8), 987-996. doi:10.1016/0016-7037(69)90108-2

Truumees, J. (2012). *Kohlenstoffisotopen-Chemostratigraphie und Faziesentwicklung in tropischen Karbonatsedimenten im Paläobaltischen Becken (Estland) während der Hirnantium-Vereisung* [Carbon isotope chemostratigraphy and depositional environment developement during Hirnantian glaciation in Baltoscandian tropical basin] PhD Thesis, Hamburg University, Hamburg.

Veizer, J., Ala, D., Azmy, K., Bruckschen, P., Buhl, D., Bruhn, F., . . . Strauss, H. (1999). 87Sr/86Sr, δ13C and δ18O evolution of Phanerozoic seawater. *Chemical Geology, CLXI*, 59-88. doi:10.1016/S0009-2541(99)00081-9

Appendix

Table 1. Ordovician $\delta^{13}C$ and $\delta^{18}O$ measurements from studied samples done by IRMS and their rock component classification. At the end of the table, bulk-rock measurements done in 2021 and also in 2015 (Ainsaar, Truumees, & Meidla, 2015) for comparison.

Count	ID1	ID2	$\delta^{13}C$ (‰V-PDB)	$\delta^{18}O$ (‰V-PDB)	Component Classification
1	K5-1	1	3.54	-3.67	Dolomitic sandstone
2	K5-1	2	3.43	-3.39	Dolomitic sandstone
3	K5-1	3	3.50	-4.25	Dolomitic sandstone
4	K5-1	4	3.23	-3.49	Dolomitic sandstone
5	K5-1	5	3.35	-2.84	Dolomitic sandstone
6	K5-1	6	3.44	-2.91	Dolomitic sandstone
7	K5-1	7	3.10	-3.70	Dolomitic sandstone
8	K5-1	8	3.63	-3.82	Dolomitic sandstone
9	K5-2	1	6.55	-5.37	Bioclastic debris
10	K5-2	2	6.43	-5.43	Bioclastic debris
11	K5-2	3	5.95	-6.27	Bioclastic debris
12	K5-2	4	5.90	-6.74	Bioclastic debris
13	K5-2	5	5.72	-6.41	Bioclastic debris
14	K5-2	6	5.60	-6.15	Bioclastic debris
15	K5-2	7	6.01	-6.78	Calcite vein
16	K5-2	8	6.00	-7.08	Calcite vein
17	K 1	1	3.81	-6.93	Bioclastic debris
18	K 1	2	3.37	-6.66	Bioclastic debris
19	K 1	3	3.99	-5.11	Bioclastic debris
20	K 1	4	4.03	-6.62	Bioclastic debris
21	K 1	5	3.81	-7.23	Bioclastic debris
22	K 1	6	3.95	-6.55	Bioclastic debris
23	K 1	7	4.13	-7.06	Bioclastic debris
24	K 1	8	4.40	-6.57	Bioclastic debris
25	K 1	9	3.74	-7.15	Bioclastic debris
26	OP	1	4.38	-5.34	Ooid
27	OP	2	4.57	-4.94	Ooid
28	OP	3	3.63	-6.29	Ooid
29	OP	4	4.94	-5.42	Ooid
30	OP	5	4.30	-5.74	Ooid
31	OP	6	4.87	-3.23	Ooid
32	OP	7	4.48	-4.51	Ooid
33	OP	8	4.07	-5.51	Ooid
34	OP	9	4.07	-5.14	Ooid
35	OP	10	3.95	-5.09	Fossil?
36	OP	11	3.95	-5.31	Matrix
37	OP	12	2.64	-5.86	Matrix
38	OP	13	2.14	-5.83	Matrix
39	OP	14	4.11	-5.17	Dark lithoclast
40	OP	15	3.31	-5.72	Dark lithoclast

41	OP	16	6.35	-4.64	Stromatoporoid
42	OP	17	4.79	-4.21	Stromatoporoid
43	OP	18	3.44	-5.10	Light lithoclast
44	OP	19	4.85	-4.01	Light lithoclast
45	OP	20	4.10	-5.45	Light lithoclast
	OP	2021	3.54	-4.76	BULK
	K5-1	2021	3.83	-2.42	BULK
	K5	2015	3.86	-2.83	BULK
	K5-2	2021	6.04	-5.69	BULK
	K5	2015	6.13	-4.89	BULK
	K1	2021	4.07	-6.40	BULK

Table 2. Silurian $\delta^{13}C$ and $\delta^{18}O$ measurements from studied sample VID-1 done by SIMS and their rock component classifications.

Count	ID	Component Classification	δ13C (‰V-PDB)	δ13C status	δ13O (‰V-PDB)	δ18O status	Total Status
1	Area1_1	Brachiopod1	8.93	Good	-3.65	Good	Good
2	Area1_2	Brachiopod1	3.53	reject	-6.13	reject	Both reject
3	Area1_3	Brachiopod1	7.10	warning	-6.09	warning	Both warning
4	Area1_4	Brachiopod1	7.03	warning	-6.02	reject	O reject
5	Area1_5	Brachiopod1	9.37	reject	-5.81	Good	C reject
6	Area1_6	Brachiopod1	9.72	reject	-6.10	Good	C reject
7	Area1_7	Brachiopod1	9.81	Good	-6.16	Good	Good
8	Area1_8	Brachiopod1	9.38	Good	-6.28	Good	Good
9	Area1_9	Brachiopod1	8.87	Good	-6.16	Good	Good
10	Area1_10	Brachiopod1	9.99	Good	-6.10	Good	Good
11	Area1_11	Brachiopod1	9.39	Good	-5.95	Good	Good
12	Area1_12	Brachiopod1	8.64	reject	-6.00	Good	C reject
13	Area1_13	Brachiopod1	8.54	Good	-6.09	warning	One warning
14	Area1_14	Matrix	1.61	reject	-6.15	reject	Both reject
15	Area1_15	Matrix	-8.25	reject	-3.21	warning	C reject
16	Area1_16	Matrix	7.89	Good	-5.26	Good	Good
17	Area1_17	Matrix	8.63	Good	-5.21	warning	One warning
18	Area1_18	Matrix	4.59	reject	-5.61	Good	C reject
19	Area1_19	Matrix	-1.23	reject	-11.42	reject	Both reject
20	Area1_20	Matrix	4.42	reject	-5.86	Good	C reject
21	Area2_1	Matrix	7.85	Good	-5.82	Good	Good
22	Area2_2	Matrix	8.93	reject	-5.88	warning	C reject
23	Area2_3	Algae	-6.44	reject	-7.27	reject	Both reject
24	Area2_4	Matrix	9.62	reject	-5.45	Good	C reject
25	Area2_5	Matrix	8.80	Good	-4.39	warning	One warning
26	Area2_6	Matrix	8.10	Good	-5.60	Good	Good
27	Area2_7	Matrix	7.76	warning	-5.67	Good	One warning

28	Area2_8	Matrix	8.46	Good	-7.36	warning	One warning
29	Area2_9	Matrix	8.46	Good	-6.12	reject	O reject
30	Area2_10	Algae	9.76	reject	-5.59	reject	Both reject
31	Area3_1	Matrix	8.96	reject	-5.93	warning	C reject
32	Area3_2	Matrix	1.08	reject	-5.04	reject	Both reject
33	Area3_3	Matrix	7.92	Good	-6.34	reject	O reject
34	Area3_4	Ostracod	5.11	reject	-5.57	reject	Both reject
35	Area3_5	Algae	9.33	Good	-5.62	reject	O reject
36	Area3_6	Matrix	8.69	Good	-5.95	reject	O reject
37	Area3_7	Ostracod	-0.51	reject	-7.13	reject	Both reject
38	Area3_8	Matrix	6.98	Good	-4.11	Good	Good
39	Area3_9	Algae	8.97	warning	-6.83	reject	O reject
40	Area3_10	Matrix	6.38	warning	-4.05	warning	Both warning
41	Area4_1	Matrix	8.51	Good	-5.45	warning	One warning
42	Area4_2	Matrix	8.54	Good	-4.97	Good	Good
43	Area4_3	Matrix	-8.43	reject	-5.90	reject	Both reject
44	Area4_4	Brachiopod2	6.50	reject	-5.41	warning	C reject
45	Area4_5	Brachiopod2	6.49	Good	-5.14	warning	One warning
46	Area4_6	Blocky calcite	2.93	reject	-8.34	reject	Both reject
47	Area4_7	Blocky calcite	7.65	reject	-5.62	reject	Both reject
48	Area4_8	Blocky calcite	6.63	Good	-6.07	warning	One warning
49	Area4_9	Blocky calcite	6.00	Good	-5.25	reject	O reject
50	Area4_10	Blocky calcite	7.73	Good	-5.77	reject	O reject
51	Area4_11	Blocky calcite	5.96	reject	-5.80	reject	Both reject
52	Area4_12	Brachiopod2	8.37	reject	-5.63	reject	Both reject
53	Area4_13	Brachiopod2	6.73	Good	-5.83	reject	O reject
54	Area4_14	Matrix	-5.62	reject	-5.53	reject	Both reject
55	Area4_15	Matrix	-5.87	reject	-5.70	reject	Both reject
56	Area4_16	Matrix	9.05	reject	-4.87	reject	Both reject
57	Area4_17	Matrix	4.36	reject	-6.84	reject	Both reject
58	Area4_18	Matrix	7.68	Good	-4.47	reject	O reject
59	Area4_19	Matrix	8.18	Good	-5.97	reject	O reject
60	Area4_20	Matrix	6.15	warning	-4.99	Good	One warning
61	Area5_1	Matrix	8.40	Good	-6.34	warning	One warning
62	Area5_2	Matrix	7.36	reject	-4.21	Good	C reject
63	Area5_3	Matrix	8.18	Good	-5.37	warning	One warning
64	Area5_4	Algae	0.52	reject	-4.49	warning	C reject
65	Area5_5	Matrix	-1.13	reject	-6.80	reject	Both reject
66	Area5_6	Matrix	2.03	reject	-3.74	Good	C reject
67	Area5_7	Algae	1.15	reject	-5.57	Good	C reject
68	Area5_8	Matrix	5.46	reject	-5.83	warning	C reject
69	Area5_9	Matrix	7.93	warning	-5.25	warning	Both warning
70	Area5_10	Matrix	8.56	Good	-5.10	reject	O reject
71	Area6_1	Matrix	4.92	reject	-5.67	Good	C reject

72	Area6_2	Brachiopod3	10.76	Good	-4.01	warning	One warning
73	Area6_3	Matrix	10.03	Good	-5.80	reject	O reject
74	Area6_4	Brachiopod3	9.55	Good	-6.28	reject	O reject
75	Area6_5	Brachiopod3	8.32	Good	-5.09	reject	O reject
76	Area6_6	Brachiopod3	8.90	Good	-4.48	Good	Good
77	Area6_7	Matrix	9.43	Good	-6.91	Good	Good
78	Area6_8	Matrix	8.36	Good	-5.88	reject	O reject
79	Area6_9	Brachiopod3	8.92	Good	-5.82	Good	Good
80	Area6_10	Matrix	9.74	Good	-4.22	warning	One warning
81	Area7_1	Matrix	5.31	reject	-3.29	Good	C reject
82	Area7_2	Matrix	8.13	Good	-4.71	Good	Good
83	Area7_3	Matrix	7.17	warning	-5.22	Good	One warning
84	Area7_4	Brachiopod4	6.48	Good	-8.22	reject	O reject
85	Area7_5	Brachiopod4	6.19	reject	-5.33	warning	C reject
86	Area7_6	Brachiopod4	5.86	warning	-5.52	warning	Both warning
87	Area7_7	Brachiopod4	-1.69	reject	-6.09	reject	Both reject
88	Area7_8	Brachiopod4	7.52	Good	-5.32	warning	One warning
89	Area7_9	Brachiopod4	7.45	Good	-5.91	reject	O reject
90	Area7_10	Brachiopod4	5.80	reject	-5.56	reject	Both reject
91	Area7_11	Brachiopod4	7.83	Good	-5.30	warning	One warning
92	Area7_12	Brachiopod4	7.83	Good	-4.94	reject	O reject
93	Area7_13	Brachiopod4	7.74	Good	-5.97	warning	One warning
94	Area7_14	Matrix	7.02	Good	-5.52	reject	O reject
95	Area7_15	Matrix	9.20	Good	-6.84	reject	O reject
96	Area7_16	Matrix	7.36	Good	-4.65	Good	Good
97	Area7_17	Matrix	8.25	Good	-5.82	reject	O reject
98	Area7_18	Matrix	8.93	Good	-3.13	reject	O reject
99	Area7_19	Algae	9.44	Good	-4.87	Good	Good
100	Area7_20	Algae	10.22	Good	-4.52	Good	Good
101	Area8_1	Ostracod	5.93	reject	-5.11	reject	Both reject
102	Area8_2	Ostracod	1.32	reject	-5.40	warning	C reject
103	Area8_3	Ostracod	2.85	reject	-5.18	warning	C reject
104	Area8_4	Matrix	8.79	Good	-5.93	Good	Good
105	Area8_5	Brachiopod5	7.43	Good	-5.58	warning	One warning
106	Area8_6	Matrix	7.50	Good	-6.35	Good	Good
107	Area8_7	Brachiopod5	9.11	Good	-5.00	warning	One warning
108	Area8_8	Brachiopod5	5.65	reject	-5.11	Good	C reject
109	Area8_9	Matrix	9.38	Good	-6.05	Good	Good
110	Area8_10	Matrix	9.02	Good	-6.35	Good	Good
111	Area9_1	Matrix	9.09	Good	-5.75	Good	Good
112	Area9_2	Matrix	7.24	Good	-5.17	reject	O reject
113	Area9_3	Brachiopod6	7.49	warning	-4.43	Good	One warning
114	Area9_4	Brachiopod6	5.15	reject	-5.94	Good	C reject
115	Area9_5	Brachiopod6	7.77	Good	-6.06	Good	Good

116	Area9_6	Brachiopod6	5.53	reject	-6.26	warning	C reject
117	Area9_7	Brachiopod6	8.74	Good	-6.11	Good	Good
118	Area9_8	Brachiopod6	9.35	Good	-6.33	Good	Good
119	Area9_9	Brachiopod6	0.87	reject	-6.95	reject	Both reject
120	Area9_10	Matrix	5.86	reject	-6.05	warning	C reject
121	Area10_1	Matrix	9.27	Good	-5.57	warning	One warning
122	Area10_2	Matrix	10.32	Good	-5.42	warning	One warning
123	Area10_3	Matrix	9.56	Good	-4.42	warning	One warning
124	Area10_4	Matrix	-1.31	reject	-4.19	warning	C reject
125	Area10_5	Algae?	9.88	Good	-8.46	reject	O reject
126	Area10_6	Algae?	1.11	reject	-5.69	reject	Both reject
127	Area10_7	Algae?	-7.31	reject	-6.02	warning	C reject
128	Area10_8	Matrix	6.32	warning	-5.81	warning	Both warning
129	Area10_9	Algae?	9.38	Good	-7.28	reject	O reject
130	Area10_10	Matrix	8.90	Good	-9.40	reject	O reject
131	Area11_1	Matrix	10.65	Good	-5.34	warning	One warning
132	Area11_2	Matrix	2.64	reject	-6.08	Good	C reject
133	Area11_3	Matrix	-3.01	reject	-4.27	Good	C reject
134	Area11_4	Matrix	7.43	Good	-3.98	warning	One warning
135	Area11_5	Matrix	10.97	Good	-5.03	reject	O reject
136	Area11_6	Matrix	8.13	reject	-4.80	warning	C reject
137	Area11_7	Matrix	9.54	Good	-5.07	reject	O reject
138	Area11_8	Matrix	8.63	Good	-5.71	reject	O reject
139	Area11_9	Matrix	3.96	reject	-5.26	warning	C reject
140	Area11_10	Matrix	8.39	Good	-5.93	Good	Good

Table 3. Silurian δ13C and δ18O measurements from studied sample VID-3 done by SIMS and their rock component classifications.

Count	ID	Component Classification	δ13C (‰V-PDB)	δ13C status	δ18O (‰V-PDB)	δ18O status	Total Status
1	Area1_1	Matrix	8.04	Good	-5.45	Good	Good
2	Area1_2	Brachiopod1?	9.30	Good	-4.37	warning	One warning
3	Area1_3	Brachiopod1?	8.44	Good	-4.48	reject	O reject
4	Area1_4	Brachiopod1?	9.09	Good	-3.84	reject	O reject
5	Area1_5	Matrix	10.00	Good	-4.26	reject	O reject
6	Area1_6	Brachiopod2?	8.51	Good	-6.34	Good	Good
7	Area1_7	Brachiopod2?	-5.97	reject	-5.05	Good	C reject
8	Area1_8	Brachiopod2?	3.42	reject	-4.86	Good	C reject
9	Area1_9	Matrix	7.18	Good	-4.44	reject	O reject
10	Area1_10	Matrix	6.11	reject	-4.09	warning	C reject
11	Area2_1	Matrix	8.36	Good	-7.91	reject	O reject
12	Area2_2	Matrix	7.73	Good	-4.12	reject	O reject
13	Area2_3	Fossil?	8.19	Good	-4.71	warning	One warning
14	Area2_4	Fossil?	7.55	reject	-4.31	reject	Both reject
15	Area2_5	Fossil?	5.88	reject	-4.83	reject	Both reject
16	Area2_6	Fossil?	-0.70	reject	-5.23	reject	Both reject
17	Area2_7	Fossil?	-6.35	reject	-4.62	reject	Both reject
18	Area2_8	Fossil?	3.25	reject	-3.93	reject	Both reject
19	Area2_9	Fossil?	3.56	reject	-4.54	reject	Both reject
20	Area2_10	Fossil?	3.29	reject	-4.45	reject	Both reject
21	Area3_1	Matrix	5.72	reject	-5.43	reject	Both reject
22	Area3_2	Matrix	9.57	Good	-4.42	warning	One warning
23	Area3_3	Matrix	4.68	reject	-5.84	reject	Both reject
24	Area3_4	Brachiopod3?	0.10	reject	-5.13	reject	Both reject
25	Area3_5	Brachiopod3?	9.47	Good	-5.40	reject	O reject
26	Area3_6	Brachiopod3?	8.56	reject	-4.48	reject	Both reject
27	Area3_7	Brachiopod3?	10.00	reject	-3.61	reject	Both reject
28	Area3_8	Brachiopod3?	8.20	Good	-3.64	reject	O reject
29	Area3_9	Brachiopod3?	-3.92	reject	-3.67	reject	Both reject
30	Area3_10	Matrix	6.62	warning	-4.68	reject	O reject
31	Area3_11	Matrix	7.45	reject	-5.46	reject	Both reject
32	Area3_12	Matrix	-9.03	reject	-5.45	reject	Both reject
33	Area3_13	Matrix	5.06	reject	-6.63	reject	Both reject
34	Area3_14	Brachiopod3?	1.89	reject	-3.65	reject	Both reject
35	Area3_15	Brachiopod3?	8.49	warning	-3.90	reject	O reject
36	Area3_16	Brachiopod3?	9.88	Good	-4.09	reject	O reject
37	Area3_17	Brachiopod3?	7.72	reject	-3.27	reject	Both reject
38	Area3_18	Brachiopod3?	9.02	Good	-3.87	reject	O reject
39	Area3_19	Brachiopod3?	8.95	Good	-4.04	reject	O reject
40	Area4_1	Matrix	-2.95	reject	-5.67	reject	Both reject

41	Area4_2	Matrix	-1.00	reject	-3.85	warning	C reject
42	Area4_3	Matrix	1.92	reject	-6.03	reject	Both reject
43	Area4_4	Algae	0.69	reject	-4.79	reject	Both reject
44	Area4_5	Matrix	4.71	reject	-3.95	Good	C reject
45	Area4_6	Matrix	8.14	Good	-4.84	warning	One warning
46	Area4_7	Algae	9.89	Good	-4.20	reject	O reject
47	Area4_8	Matrix	3.63	reject	-6.46	reject	Both reject
48	Area4_9	Matrix	8.57	warning	-7.08	warning	Both warning
49	Area4_10	Matrix	-10.55	reject	-7.21	reject	Both reject
50	Area5_1	Matrix	3.40	reject	-4.62	Good	C reject
51	Area5_2	Matrix	4.22	reject	-4.02	reject	Both reject
52	Area5_3	Matrix	8.87	warning	-3.55	reject	O reject
53	Area5_4	Matrix	-4.34	reject	-4.92	reject	Both reject
54	Area5_5	Brachiopod4	13.04	warning	-4.72	Good	One warning
55	Area5_6	Brachiopod4	13.48	Good	-4.17	Good	Good
56	Area5_7	Brachiopod4	12.04	Good	-4.18	Good	Good
57	Area5_8	Matrix	3.31	reject	-5.70	reject	Both reject
58	Area5_9	Matrix	-6.84	reject	-5.61	Good	C reject
59	Area5_10	Matrix	7.60	reject	-4.40	reject	Both reject

Table 4. LA-ICP-MS measurements (ppm) averages for each corresponding micro-drilled hole on studied sample OP.

ID	Mg	Al	Si	P	Mn	Fe	Sr	Y	Ba	La	Ce	Pr	Nd	Sm	Eu	Gd	Ho	Pb	U
OP-1/2	1622.75	668.33	1780.00	71.75	572.25	1385.00	174.35	8.01	4.21	5.60	8.28	1.07	4.89	0.87	0.24	1.20	0.18	13.59	0.14
OP-3	1405.33	321.17	946.67	48.43	965.00	645.33	121.07	4.96	3.22	4.99	7.73	0.91	3.47	0.52	0.16	0.96	0.11	4.33	0.10
OP-4	2059.67	915.00	3100.00	56.40	774.33	2404.00	217.67	6.10	5.20	4.52	7.19	0.91	3.69	0.58	0.16	0.79	0.14	22.80	0.14
OP-5	1933.67	1194.67	3630.00	71.33	896.33	1326.33	186.97	6.09	5.59	5.61	8.39	1.04	3.98	0.65	0.18	0.91	0.12	8.55	0.15
OP-6	1982.67	1355.33	4046.67	87.33	739.67	1620.50	179.23	6.19	5.98	4.08	6.09	0.81	3.08	0.43	0.16	0.73	0.12	45.59	0.30
OP-7	2496.33	1621.33	4336.67	77.33	663.33	4410.67	292.13	6.73	7.73	4.05	6.62	0.81	3.17	0.45	0.13	0.86	0.14	37.34	0.21
OP-8	1950.00	923.33	2476.67	60.67	848.67	2436.67	207.33	6.14	5.36	5.27	7.83	0.98	4.00	0.59	0.20	1.04	0.11	32.67	0.12
OP-9	2216.00	1634.67	4796.67	101.70	967.00	12883.33	202.50	5.92	6.61	4.69	7.42	0.95	3.80	0.62	0.19	0.80	0.12	119.00	0.27
OP-10	2236.67	1030.67	3310.00	57.27	864.67	731.33	241.03	6.59	5.91	4.58	6.63	0.84	3.28	0.45	0.15	0.97	0.14	2.46	0.16
OP-11	2419.67	1047.57	3094.00	86.60	611.13	1671.00	286.20	6.43	5.09	3.71	5.56	0.74	3.09	0.58	0.17	0.89	0.14	12.62	0.13
OP-12	2948.33	506.30	1970.00	59.13	1445.33	953.00	274.20	7.40	4.37	6.74	9.26	1.20	4.83	0.88	0.23	1.20	0.18	3.26	0.17
OP-13	2947.00	2440.00	7410.00	59.15	1322.00	1602.00	168.40	7.31	11.40	6.79	9.68	1.19	5.05	0.86	0.26	1.14	0.18	3.66	
OP-14	40271.0	1339.00	4453.33	129.67	1783.33	205823.33	183.97	10.38	7.52	8.32	12.25	1.67	7.29	1.23	0.34	1.75	0.25	1726.97	0.28
OP-15	80753.0	2486.67	7766.67	114.67	2550.33	15786.67	127.33	12.50	10.01	10.91	17.78	2.27	9.02	1.63	0.45	2.11	0.31	67.93	0.38
OP-16	2103.00	0.00	366.50	29.15	1377.33	463.00	298.57	0.91	2.27	1.32	1.37	0.15	0.49	0.00	0.05	0.31	0.00	7.65	0.09
OP-17	2964.00	5.22	0.00	38.50	528.67	177.33	320.80	2.57	3.17	2.16	3.14	0.38	1.60	0.20	0.10	0.51	0.05	0.83	0.02
OP-18	61107.5	1427.00	7937.50	61.50	2114.50	12230.00	199.78	9.71	7.13	10.35	16.30	2.03	7.97	1.39	0.39	1.75	0.24	61.43	0.16
OP-19	2119.33	1170.00	5176.67	79.80	757.00	1095.33	203.73	4.83	4.82	3.89	5.74	0.71	2.82	0.39	0.12	0.78	0.10	6.15	0.14
OP-20	9273.67	2514.67	6870.00	84.00	1362.33	5000.00	337.77	6.32	9.95	6.14	9.20	1.13	4.73	0.72	0.23	1.01	0.12	61.48	0.21

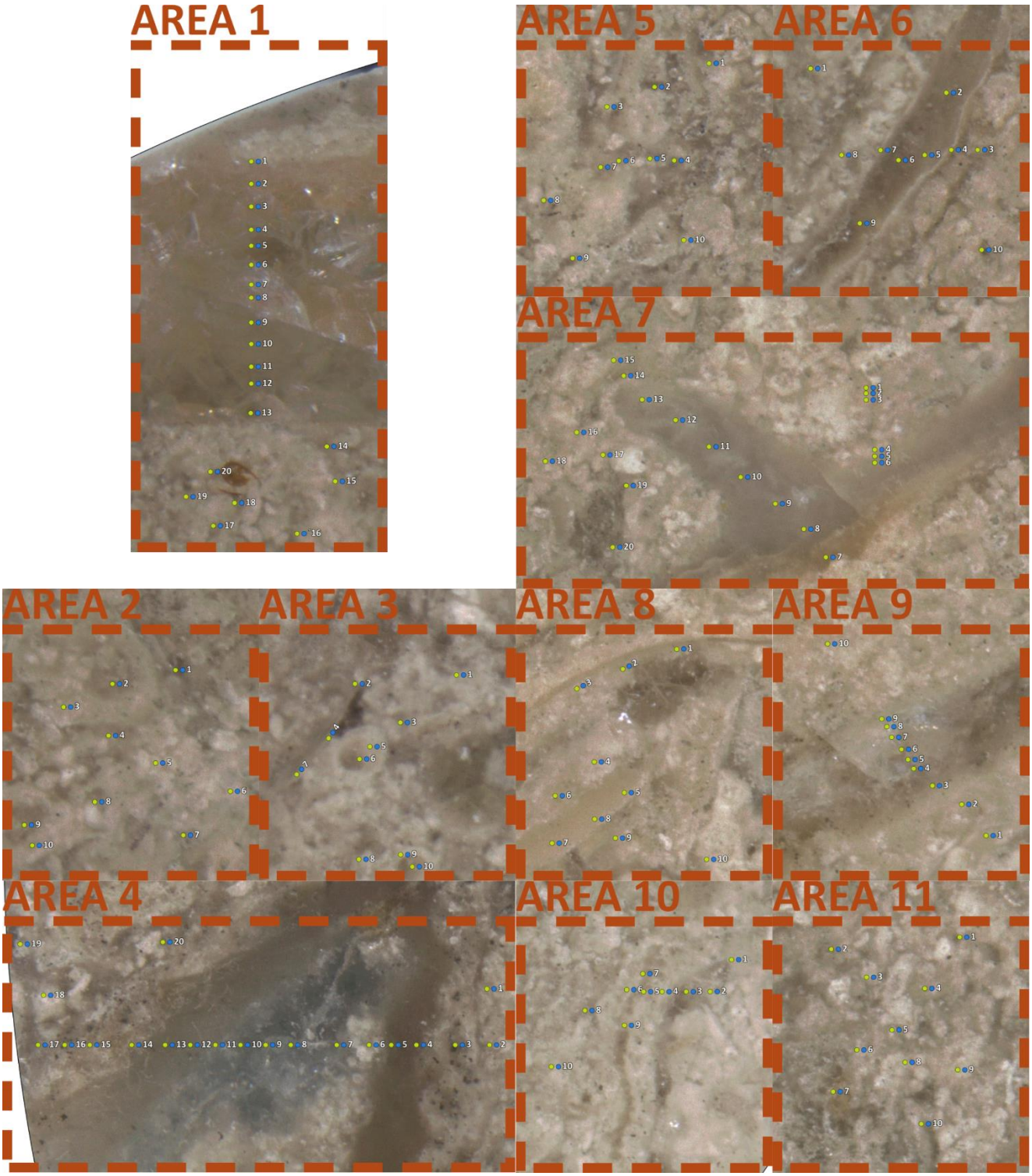

Figure 24. Studied sample VID-1, close-ups of defined areas with assigned SIMS measurement spots.

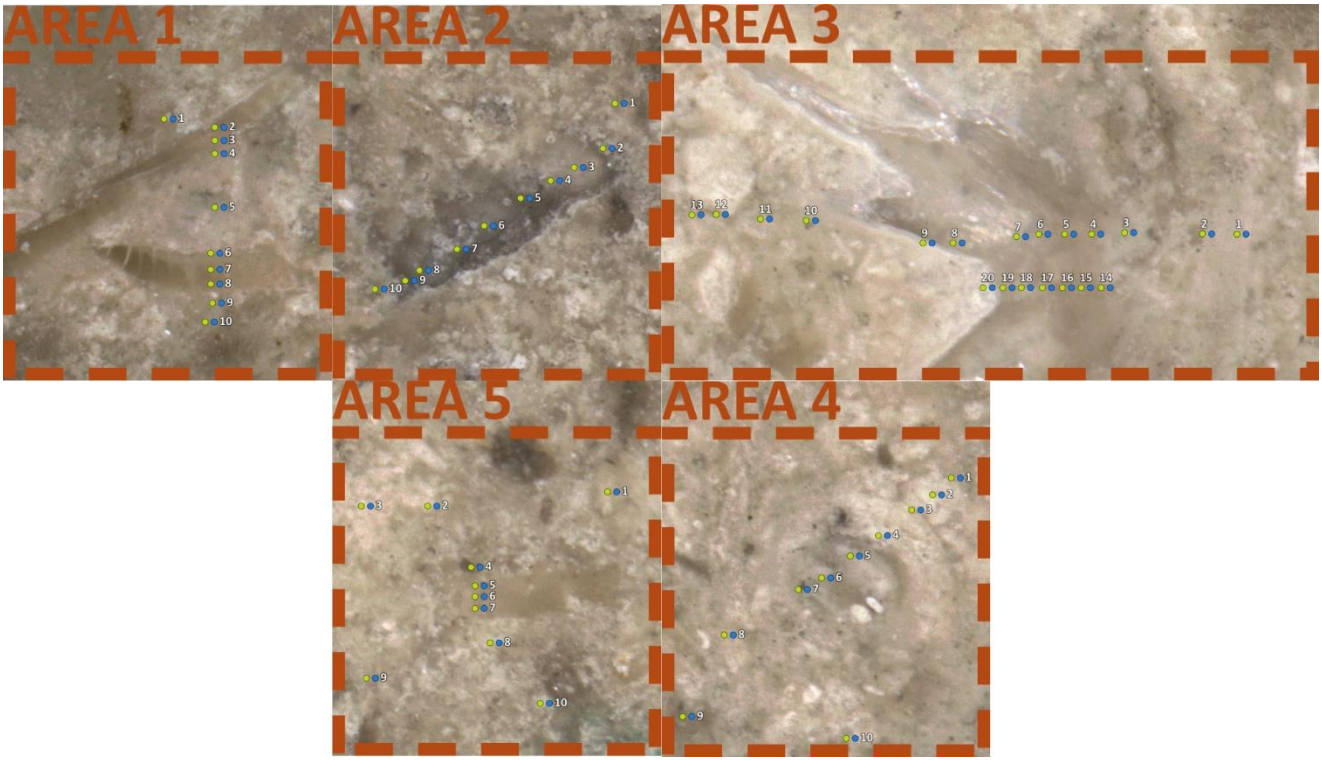

Figure 25. Studied sample VID-3, close-ups of defined areas with assigned SIMS measurement spots.

Non-exclusive licence to reproduce the thesis and make the thesis public

I, Imre Andreas Martin,

1. grant the University of Tartu a free permit (non-exclusive licence) to

reproduce, for the purpose of preservation, including for adding to the DSpace digital archives until the expiry of the term of copyright, my thesis

Palaeozoic carbon isotope anomalies and sample-scale component analysis

Supervised by Leho Ainsaar ja Aivo Lepland,

reproduce, for the purpose of preservation, including for adding to the DSpace digital archives until the expiry of the term of copyright, my thesis

2. I grant the University of Tartu a permit to make the thesis specified in point 1 available to the public via the web environment of the University of Tartu, including via the DSpace digital archives, under the Creative Commons licence CC BY NC ND 4.0, which allows, by giving appropriate credit to the author, to reproduce, distribute the work and communicate it to the public, and prohibits the creation of derivative works and any commercial use of the work until the expiry of the term of copyright.

3. I am aware of the fact that the author retains the rights specified in points 1 and 2.

4. I confirm that granting the non-exclusive licence does not infringe other persons' intellectual property rights or rights arising from the personal data protection legislation.

Imre Andreas Martin

27.05.2022